

# Strong influence of trees outside forest in regulating microclimate of intensively modified Afromontane landscapes

Iris J. Aalto<sup>1</sup>, Eduardo E. Maeda<sup>1</sup>, Janne Heiskanen<sup>1,2</sup>, Eljas K. Aalto<sup>3</sup>, Petri K. E. Pellikka<sup>1</sup>

<sup>1</sup>Department of Geosciences and Geography, University of Helsinki, P.O. Box 64, FI-00014, Helsinki, Finland

<sup>2</sup>Institute for Atmospheric and Earth System Research, Faculty of Science, University of Helsinki, Finland

<sup>3</sup>Department of Economics, Turku School of Economics, 20014 University of Turku, Finland

Correspondence to: Iris Aalto (iris.aalto@helsinki.fi)

**Abstract.** Climate change is expected to have detrimental consequences on fragile ecosystems, threatening biodiversity as well as food security of millions of people. Trees are likely to play a central role in mitigating these impacts. The microclimatic conditions below tree canopies usually differ substantially from the ambient macroclimate, as vegetation can buffer temperature changes and variability. Trees cool down their surroundings through several biophysical mechanisms, and the cooling benefits occur also with trees outside forest. The aim of this study was to examine the effect of canopy cover on microclimate in an intensively modified Afromontane landscape in Taita Taveta, Kenya. We studied temperatures recorded by 19 microclimate sensors under different canopy covers, and land surface temperature (LST) estimated by Landsat 8 thermal infrared sensor. We combined the temperature records with high-resolution airborne laser scanning data to untangle the combined effects of topography and canopy cover on microclimate. We developed four multivariate regression models to study the joint impacts of topography and canopy cover on LST. The results showed a negative linear relationship between canopy cover percentage and daytime mean ( $R^2 = 0.65$ ) and maximum ( $R^2 = 0.75$ ) temperatures. Any increase in canopy cover contributed to reducing temperatures. The average difference between 0% and 100% canopy cover sites was 5.27 °C in mean temperatures and 10.2 °C in maximum temperatures. Canopy cover reduced LST on average by 0.05 °C/%CC. The influence of canopy cover on microclimate was shown to vary strongly with elevation and ambient temperatures. These results demonstrate that trees have substantial effect on microclimate, but the effect is dependent on macroclimatic ~~conditionse~~, highlighting the importance of maintaining tree cover particularly in warmer conditions. Hence, we demonstrate that trees outside forests can increase climate change resilience in fragmented landscapes, having strong potential for regulating regional and local temperatures.

## Keywords

Agroforestry, airborne laser scanning, canopy cover, land surface temperature, Landsat 8, microclimate

31 **1. Introduction**

32 Climate change poses an imminent threat to the rich biodiversity and frequently found fragile socio-economic conditions  
33 that characterize Afromontane ecosystems and their surroundings. In these regions, climate warming is mostly driven by  
34 land use and land cover change (LULCC) (IPCC, 2018; Pellikka and Hakala, 2019; Abera et al., 2020). Agricultural  
35 expansion, in particular, has caused rapid loss of tropical forests (FAO, 2016). Forests are essential in mitigating climate  
36 warming, due to their role in especially the carbon and water cycles (Beer et al. 2010; Ellison et al. 2017; De Frenne et  
37 al. 2019).

38 Currently, forests cover approximately 4 billion hectares of the Earth’s surface (FAO, 2016). [Forests are often defined as](#)  
39 [a land area of at least 0.5 hectares with a minimum canopy cover of 10 % and trees higher than 5 m \(FAO, 2015\).](#) Trees  
40 that are not part of a forest are commonly called “trees outside forest” (TOF) and, by the definition of FAO (2000), include  
41 trees on farmland, in cities, and in other locations not defined as forest. Forests and TOF provide vital ecosystem services  
42 including water regulation, air purification, carbon sequestration, and climate regulation ([Chakravarty et al., 2019; Kuyah](#)  
43 [et al., 2019; Skole et al., 2021](#)). They are also a source of goods for humans, [such as food and timber \(Thijs et al., 2015;](#)  
44 [Martínez Pastur et al., 2018; Chakravarty et al., 2019\).](#) As global forest cover decreases, the importance of TOF will  
45 [increase in biodiversity conservation and ecosystem service provision \(Mace et al. 2012; Mendenhall et al. 2016\), and](#)  
46 [TOF can be beneficial in reducing the pressure on native forests \(Ilyama et al., 2014; Chakravarty et al., 2019\).](#) For  
47 [example, in Taita Hills in Kenya, TOF make up a remarkable amount of the area’s total aboveground carbon and play an](#)  
48 [important part in carbon sequestration in the area \(Pellikka et al., 2018\), especially because Taita Hills have experienced](#)  
49 [massive indigenous forest loss since 1950’s \(Pellikka et al., 2009\). Forest loss is a major threat to biodiversity, as Taita](#)  
50 [Hills are identified as an important biodiversity hotspot \(Pellikka et al., 2013; Thijs et al., 2015\). Biodiversity is considered](#)  
51 [fundamental for the provision of ecosystem services \(Mace et al., 2012\).](#)

52 Many ecosystem services, such as nutrient cycling and pollination, occur in the understories, where tree canopies create  
53 the appropriate microclimates essential for these processes (De Frenne et al., 2013). The term “microclimate” describes  
54 the climatic conditions near the ground or along the vertical forest profile, [experienced by terrestrial organisms with a](#)  
55 [scale from centimeters to meters \(De Frenne et al., 2019; Zellweger et al., 2019\).](#) In contrast to free air temperatures,  
56 which are highly controlled by elevation and atmospheric processes, temperatures close to the ground are primarily  
57 affected by topographic factors and vegetation structures that produce local microclimates through shading, mixing of  
58 air, and evapotranspiration ([Geiger, 1980; Das et al., 2015; Zellweger et al., 2020](#)). [Climatic conditions below forest](#)  
59 [canopies can vary spatially within the forest \(Chen et al., 1999\) and differ substantially from the ambient macroclimate;](#)  
60 [this difference is referred to as microclimatic buffering \(Ewers and Banks-Leite, 2013; Zellweger et al., 2020\).](#) Climatic

61 conditions below forest canopies can differ substantially from the ambient macroclimate. Furthermore, they can vary  
62 spatially within the forest (Chen et al., 1999). This variability has different magnitudes at different latitudes: for example,  
63 tropical forests experience the strongest cooling effect (Li et al., 2015; Wanderley et al., 2019). The temperature buffering  
64 provided by tree cover may protect ecosystems from climate change consequences (Zomer et al., 2016; Ellison et al.,  
65 2017; De Frenne et al., 2019; Wanderley et al., 2019), but the magnitude of the buffering is affected by the forest area  
66 (Ewers and Banks-Leite, 2013). In time, forest microclimates will likely warm like the macroclimate around them, and  
67 fragmentation may accelerate this process (Ewers and Banks-Leite, 2013; Li et al., 2016).

68 ~~Studies about forests' response to climate warming have primarily focused on the macroscale.~~ Despite wide recognition  
69 of the vital role microclimates play, ~~studies about tropical forests' response to climate warming have primarily focused~~  
70 ~~on the macroscale~~ (Belsky et al., 1989; De Frenne et al., 2019; Wild et al., 2019). ~~Weather stations that commonly~~  
71 ~~measure free air temperatures at 1.5 meters height do not capture microclimatic conditions that are ecologically more~~  
72 ~~relevant to terrestrial organisms~~ (Potter et al., 2013; Wild et al., 2019; Maclean et al., 2021). Further, microclimate may  
73 be a better indicator of how well forests mitigate climate change than macroclimate (De Frenne et al., 2013). Due to the  
74 importance of microclimatic conditions for the survival of tropical species facing climate change, below-canopy  
75 microclimates warrant further investigation (Potter et al., 2013; Jucker et al., 2018; De Frenne et al., 2021). ~~In our study~~  
76 ~~area in Kenya, temperatures are expected to increase by 2–4 °C by the end of the century (Adhikari et al., 2015), and~~  
77 ~~changes in precipitation, that will increase the moisture stress of crops, are projected (MoALF, 2016). Dry spells, heat~~  
78 ~~stress and extreme rain events pose a threat to the area's agricultural production. These phenomena cause crop failure and~~  
79 ~~low yields, and hence affect the livelihoods of people (Adhikari et al., 2015; MoALF 2016). Farmers have already noticed~~  
80 ~~climate fluctuations that affect both crops and livestock in the area (Mwalusepo et al., 2015).~~

81  
82 ~~However,~~ ~~M~~microclimatic studies require extensive field measurements, making them sometimes unpractical or  
83 imprecise in larger scale applications (Prata et al., 1995). Alternatively, measuring satellite-derived land surface  
84 temperature (LST) proves useful when point-wise field measurements are insufficient, given the high spatial coverage of  
85 spaceborne LST and the strong correlation between LST and air temperature (Jin and Dickinson, 2010; Li et al., 2013).  
86 ~~These two measurements differ in their physical principles: air temperature is the kinetic temperature of the air, whereas~~  
87 ~~LST is defined as the radiometric temperature recorded by a satellite sensor in a scale of the sensor's pixel size (Jin and~~  
88 ~~Dickinson, 2010). Various factors affect LST: atmospheric conditions, water content of the surface, topography and~~  
89 ~~canopy cover control the energy exchange processes (Goward and Hope, 1989; Nemani et al., 1993), which makes~~  
90 ~~accurate estimation of LST remains a challenge (Simó et al., 2018; Li et al., 2013). Vegetation density has a strong negative~~

91 [relationship with LST due to evapotranspiration causing increased latent heat loss from the canopy \(Goward et al., 1985;](#)  
92 [Goward and Hope, 1989; Nemani and Running, 1997\). Canopies' cooling effect has different magnitudes at different](#)  
93 [latitudes: for example, tropical forests experience the strongest cooling effect \(Li et al., 2015; Wanderley et al.,](#)  
94 [2019\). However, LST cannot provide information in the smallest relevant scales, such as organism level \(Potter et al.,](#)  
95 [2013; Jucker et al., 2018\). Due to the various factors affecting LST, accurate estimation remains a challenge \(Simó et al.,](#)  
96 [2018; Li et al., 2013\). Nevertheless, the complexity of the issue with climate change requires attention at both spatial](#)  
97 [resolutions.](#)

98 In remote sensing of vegetation, common outputs in previous research are land cover and land use types or vegetation  
99 indices, such as the normalized vegetation index (NDVI) or leaf area index (LAI) (Nemani et al., 1993; Kim 2013; He et  
100 al., 2019). However, airborne laser scanning (ALS) has proven to be a more effective method for computing structural  
101 variables, such as above-ground biomass, canopy height, and canopy cover (Griffin et al., 2008; Heiskanen et al., 2015a;  
102 Heiskanen et al., 2015b; Pellikka et al., 2018; Jucker et al., 2018). Canopy cover (CC) describes the proportion of the  
103 forest floor covered by the vertical projection of the tree crowns (Korhonen et al., 2006) and it is the most important  
104 variable used in defining forests or other land with tree cover (FAO, 2015). ALS can assess tree cover over large areas  
105 more precisely than field measurements can. Hence, when ALS is combined with either field-based or remotely sensed  
106 temperatures, we can study the influence of trees on temperature in a new way of that is both nuanced and large scale.

107 [The complexity of the issue with climate change requires attention at both spatial resolutions.](#)

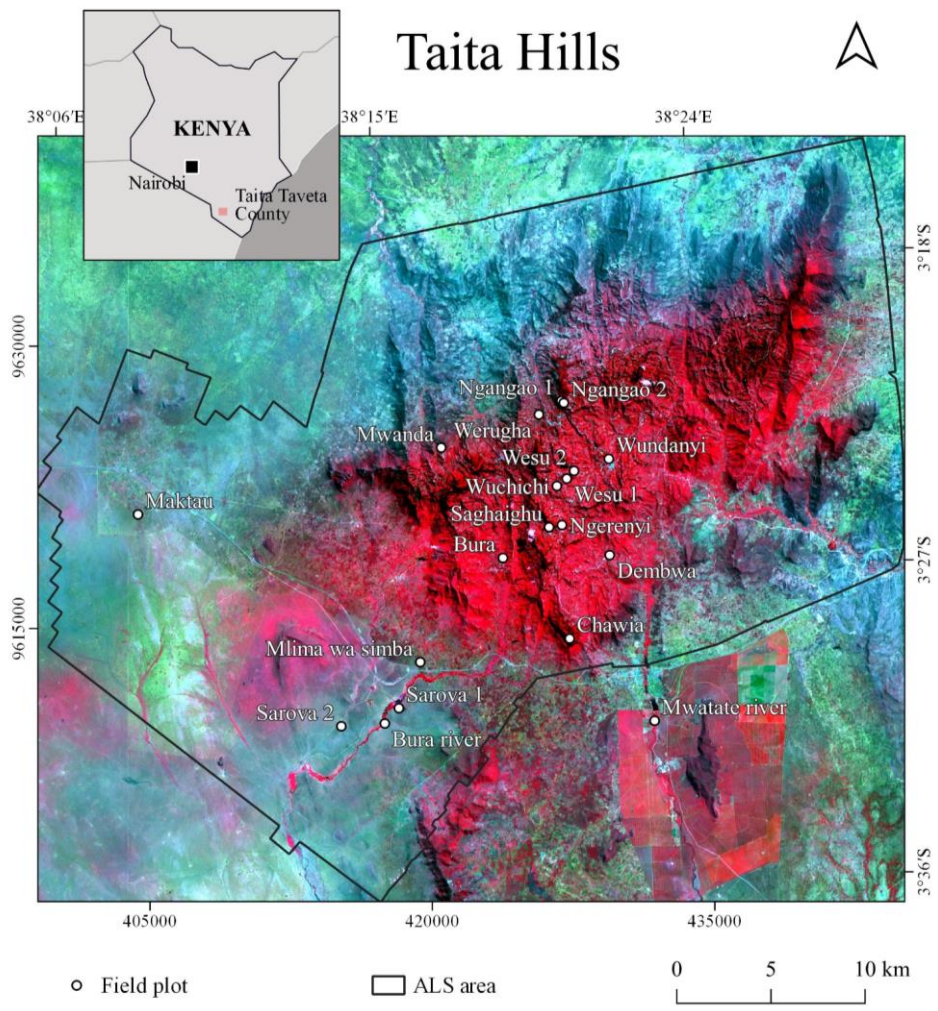
108 The primary objective of this study was to examine how different levels of CC can contribute to lower temperatures and  
109 more stable microclimates across a highly heterogeneous Afromontane landscape in Kenya. We based our analysis on  
110 micro-climatological measurements and CC estimates retrieved from ALS data. Microclimate sensors cannot entirely  
111 capture the spatial variability of temperatures, especially in heterogeneous landscapes. Therefore, we used satellite  
112 thermal data to provide a comprehensive and spatially continuous representation of the relationship between CC and  
113 temperature.

## 115 2. Materials and methods

### 116 2.1 Study area

117 The Taita Hills are located in the Taita-Taveta County in the Coast Province in southern Kenya ([3° 25' S, 38° 20' E](#)),  
118 approximately 200 km from Mombasa and 360 km from the capital city Nairobi. The study area comprises of the Taita  
119 Hills and the lowland areas of Maktau, LUMO Community Wildlife Sanctuary and Taita Hills Wildlife Sanctuary that

120 have been laser scanned by [the](#) University of Helsinki (Fig. 1). The elevation in the study area varies from 640 m in the  
121 lowlands to the highest peak of the hills, Vuria, at 2208 m. Climate is mainly semi-arid. According to the Kenya Ministry  
122 of Agriculture, Livestock and Fishery (MoALF), annual precipitation averages 650 mm, but differences between hills and  
123 lowlands are notable: lowlands receive 500 mm annually compared to 1500 mm in the hills. Two rainy seasons control  
124 the climate and growing seasons: long rains from March to June, and short rains from October to December (Pellikka et  
125 al., 2013), while months from January to March are a short hot dry season and months from June to October long cool  
126 dry season (Wachiye et al., 2020). Mean temperature in the lowlands is 23 °C and in the hills 18 °C (MoALF, 2016).  
127 Vegetation varies from dry savanna and shrubland in the lowlands dominated by *Vachellia ssp.* and *Commiphora ssp.*  
128 tree species to indigenous cloud forests in the hilltops. Small indigenous forest fragments, exotic tree plantations, and  
129 intensive agriculture dominate the landscape in the hills. Agroforestry practices are typical, which increases cropland CC.  
130 ~~TOF make up a remarkable amount of the area's total aboveground carbon and play an important part in carbon~~  
131 ~~sequestration in the area (Pellikka et al., 2018), especially because Taita Hills have experienced massive indigenous forest~~  
132 ~~loss since 1950's (Pellikka et al., 2009). Forest loss is a major threat to biodiversity, as Taita Hills are identified as an~~  
133 ~~important biodiversity hotspot (Pellikka et al., 2013; Thijs et al., 2015).~~  
134 ~~With climate change, temperatures in Kenya are expected to increase by 2–4 °C by the end of the century (Adhikari et~~  
135 ~~al., 2015), and changes in precipitation, that will increase the moisture stress of crops, are projected (MoALF, 2016). Dry~~  
136 ~~spells, heat stress and extreme rain events pose a threat to the area's agricultural production. These phenomena cause crop~~  
137 ~~failure and low yields, and hence affect the livelihoods of people (Adhikari et al., 2015; MoALF 2016). Farmers in the~~  
138 ~~area have already noticed climate fluctuations that affect both crops and livestock (Mwalusepo et al., 2015).~~



139

140 **Figure 1:** Field plots with microclimate sensors in Taita Taveta County, Kenya. [ALS refers to airborne laser scanning.](#)

141 The base map is a false color Landsat 8 OLI image from July 4, 2019.

142

143 **2.2 Airborne laser scanning data**

144 We applied an ALS-based Digital Elevation Model (DEM) raster at 1 m resolution and a CC raster at 30 m resolution.  
145 The ALS data for the hills were acquired in February 2014 and February 2015, and the data for lowland areas in March  
146 2014. The mean pulse density of the ALS data in the hills was 3.1 pulses/m<sup>2</sup> and mean return density 3.4 returns/m<sup>2</sup>, for  
147 the lowlands the pulse density was 1.04 pulses/m<sup>2</sup>. The ALS data used in this study are described in detail in Adhikari et  
148 al. (2017) and Amara et al. (2020) with the description of pre-processing and derivation of DEM and CC rasters.

149 We resampled the DEM to 30 m resolution to fit to the spatial resolution of the Landsat 8 image, and utilized it to derive  
150 topographic factors slope degree (°) and aspect (°) using ArcGIS Pro spatial analyst tools.

### 151 2.3 Microclimatological field measurements

152 Based on the CC raster derived from the ALS data, we selected a total of 19 field plots representing different CC levels  
153 (Table 1). In the plots, we installed TOMST TMS-4 microclimate sensors to measure temperature at three different  
154 heights: soil at 6 cm below ground, surface at 2 cm above ground, and air temperature at 15 cm above ground ( $T_{\text{soil}}$ ,  $T_{\text{surface}}$   
155 and  $T_{\text{air}}$ , respectively) (Wild et al., 2019). ~~from June 13 to July 10, 2019. The sensors were deployed in places that were~~  
156 ~~as flat as possible to reduce the effect of slope, and that received both sunlight and shade during the day with the changing~~  
157 ~~sun angles. In high CC sites, the sensors were shaded most of the day, while in the open areas, the sensors were exposed~~  
158 ~~to sunlight all day.~~

159 The sensors measured parameters every 15 minutes ~~from June 13 to July 10, 2019~~. We calculated daytime temperature  
160 aggregates between sunrise and sunset, local time 06.30–18.30 UTC + 3h. We calculated maxima as the mean of daily  
161 maxima, and minimum temperatures as the mean of minimum temperatures based on the 24 hour cycle.

162 To isolate the influence of CC on microclimate, we quantified and later removed the effect of topography, such as  
163 elevation (m) and slope (°), on temperature. We examined the relationships between the variables first with Pearson's  
164 correlation using elevation, slope and CC as explanatory variables in a multiple regression model. Elevation and CC were  
165 the only statistically significant variables. We corrected the daytime mean temperatures according to the altitudinal lapse  
166 rates, which were 7.26 °C km<sup>-1</sup> for soil temperature ( $T_{\text{soil}}$ ), 8.09 °C km<sup>-1</sup> for surface temperature ( $T_{\text{surface}}$ ) and 8.06 °C km<sup>-1</sup>  
167 <sup>1</sup> for air temperature ( $T_{\text{air}}$ ). ~~In the case of diurnal analysis, we applied separate lapse rates for each hour that were derived~~  
168 ~~from the regression analyses. The lapse rates were 6.1 °C–8.2 °C km<sup>-1</sup> in  $T_{\text{soil}}$ , 3.8 °C–10.4 °C km<sup>-1</sup> in  $T_{\text{surface}}$ , and 3.3 °C–~~  
169 ~~10.2 °C km<sup>-1</sup> in  $T_{\text{air}}$ . In the case of diurnal analysis, we applied separate lapse rates for each hour. These varied from 6.1~~  
170 ~~°C to 8.2 °C km<sup>-1</sup> in  $T_{\text{soil}}$ , 3.8 °C to 10.4 °C km<sup>-1</sup> in  $T_{\text{surface}}$ , and 3.3 °C to °C km<sup>-1</sup> in  $T_{\text{air}}$ .~~ To find the relationships between  
171 temperature, CC and topographic variables, we conducted statistical analyses, including descriptive statistics, linear

172 regression and Pearson's correlation. [We used standard deviation \(SD\) to describe the variability of temperatures.](#) We  
 173 used RStudio (R Core Team, 2019) for all statistical analyses.

174 [The ALS data was 4–5 years older than the field measurements. Moreover, the ALS data was collected during the short](#)  
 175 [dry season, in contrast to the field measurements, which we carried out during the start of the long dry season in June](#)  
 176 [2019. To address the mismatch between the data collection dates, we acquired hemispherical photography at each field](#)  
 177 [plot for validating the CC raster. The differences in CC were not statistically significant and we considered the estimates](#)  
 178 [consistent enough for proceeding the analysis using CC from ALS. In the case of Mwatate river plot, CC was retrieved](#)  
 179 [by hemispherical photography only, because the plot was outside of the ALS coverage. The methodology is described in](#)  
 180 [Appendix A.](#)~~Because the ALS data was 4–5 years older than the field measurements, we acquired hemispherical~~  
 181 ~~photography at each field plot for validating the CC raster. Moreover, the ALS data was collected during the short dry~~  
 182 ~~season, in contrast to the field measurements, which we carried out during the start of long dry season in June 2019. For~~  
 183 ~~Mwatate river plot, CC was retrieved by hemispherical photography only, as the plot was laying outside of the ALS~~  
 184 ~~coverage. The methodology is described in the supplementary material.~~

Site	CC %	Elevation, m	Description
Bura	68	1095	Parkland by school campus
Bura river	79	880	Riverine forest
Chawia	97	1562	Indigenous forest
Dembwa	13	1083	Agroforestry
Maktau	19	1044	Bushland
Mlima wa simba	8	923	Bushland
Mwanda	2	1653	Bushland
Mwatate river	63	884	Riverine forest
Ngangao 1	94	1775	Indigenous forest
Ngangao 2	77	1778	Eucalyptus forest
Ngerenyi campus	44	1572	Macadamia plantation
Saghaighu	16	1611	Agroforestry
Sarova 1	0	901	Bushland
Sarova 2	0	900	Grassland
Werugha	8	1613	Macadamia plantation



Wesu 1	53	1642	Forest edge
Wesu 2	0	1562	Open maize field
Wuchichi	36	1595	Agroforestry
Wundanyi	31	1372	Riverside bushland

185 **Table 1:** Names, canopy cover (CC) percentages, elevations and descriptions of field plot sites.

## 186 2.4 Land sSurface fTemperature

187 To observe the effect of CC on temperature in Taita Taveta County, we applied Landsat 8 OLI thermal infrared sensor  
 188 (TIRS) satellite image data, downloaded from USGS Earth Explorer (<https://earthexplorer.usgs.gov/>). The bands 10 and  
 189 11 of TIRS provide thermal infrared imagery in a resolution of 100 m, but we resampled the band to 30 m to concert with  
 190 the OLI images. The image used in the study was a Level-1 scene obtained on July 4, 2019 at approximately 10:30 UTC  
 191 + 3h with solar azimuth angle of 45.6° and solar elevation angle of 52.1°. The cloud cover of the whole scene was 11.67  
 192 %; there was no completely cloudless scene over the study area for the timing of the field measurements.

193 Several methods have been developed to retrieve LST from Landsat 8. Unfortunately, shortly after the launch of Landsat  
 194 8 in 2013, a stray light problem was detected with TIRS band 11, and it was not recommended by United States Geological  
 195 Survey (USGS) to apply for scientific purposes (USGS, 2017). ~~In order to result in a topographically corrected LST~~  
 196 ~~product, We~~ applied the workflow by Ndossi and Avdan (2016) ~~and (Fig. 2). We~~ used the single channel (SC) method  
 197 by Jiménez-Muñoz and Sobrino (2003) to calculate LST, because SC method needs only one thermal infrared channel,  
 198 and land surface emissivity (LSE) and water vapor content as parameters. ~~Using only one channel may introduce~~  
 199 ~~uncertainty in LST estimations: for Landsat 8 band 10, Jiménez-Muñoz et al. (2014) reported RMSE = 1.5 K, while in~~  
 200 ~~Ndossi and Avdan (2016) the RMSE = 3.06 °C. Nevertheless, SC method is most accurate for sensors with effective~~  
 201 ~~wavelengths near to 11 μm (Jiménez-Muñoz et al., 2014), the wavelength of Landsat 8 band 10 being 10.6–11.19 μm.~~

202 ~~We calculated LSE using the algorithm based on the NDVI image, where pixels were given pre-defined emissivity values~~  
 203 ~~based on the NDVI derived from the red, green and infrared bands. Please refer to Ndossi and Avdan (2016) for more~~  
 204 ~~details. Water vapor content at the time of the satellite overpass was 1.7 g cm<sup>-2</sup>, and was calculated with Eq. (1) using the~~  
 205 ~~relative humidity and temperature data obtained from the local weather station:~~

$$206 \quad w = 0.0981 \times \left\{ 10 \times 0.6108 \times \exp \left[ \frac{17.27 \times (T_0 - 273.15)}{237.3 + (T_0 - 273.15)} \right] \times RH \right\} + 0.1679 \quad (1)$$

207 ~~where  $w$  = water vapor content,  $T_0$  = air temperature and  $RH$  = relative humidity.~~

208 ~~The SC formula is shown in Eq. (2+):~~

$$T_s = \gamma \left[ \frac{1}{\varepsilon} (\Psi_1 L_{sen} + \Psi_2) + \Psi_3 \right] + \delta \quad (24)$$

$$\gamma = \frac{T_{sen}^2}{b_\gamma L_{sen}} \quad (32)$$

$$\delta = T_{sen} - \frac{T_{sen}^2}{b_\gamma} \quad (43)$$

where  $T_s$  = LST,  $\gamma$  = parameter depending on Eq. (32),  $\delta$  = parameter depending on Eq. (43),  $\varepsilon$  = land surface emissivity,  $L_{sen}$  = top of atmosphere spectral radiance ( $\text{W sr}^{-1} \text{m}^{-2} \mu\text{m}^{-1}$ ),  $b_\gamma = 1324 \text{ K}$  for Landsat 8 band 10, and  $T_{sen}$  = at sensor brightness temperature (K). We obtained the atmospheric parameters  $\Psi_1$ ,  $\Psi_2$  and  $\Psi_3$  with Eq. (54):

$$\begin{bmatrix} \Psi_1 \\ \Psi_2 \\ \Psi_3 \end{bmatrix} = \begin{bmatrix} c_{11} & c_{12} & c_{13} \\ c_{21} & c_{22} & c_{23} \\ c_{31} & c_{32} & c_{33} \end{bmatrix} \begin{bmatrix} \omega^2 \\ \omega \\ 1 \end{bmatrix} \quad (54)$$

According to Jiménez-Muñoz, et al. (2014), the coefficients for atmospheric parameters for Landsat 8 TIRS are as in Eq. (65):

$$c = \begin{bmatrix} 0.04019 & 0.02916 & 1.01523 \\ -0.38333 & -1.50294 & 0.20324 \\ 0.00918 & 1.36072 & -0.27514 \end{bmatrix} \quad (65)$$

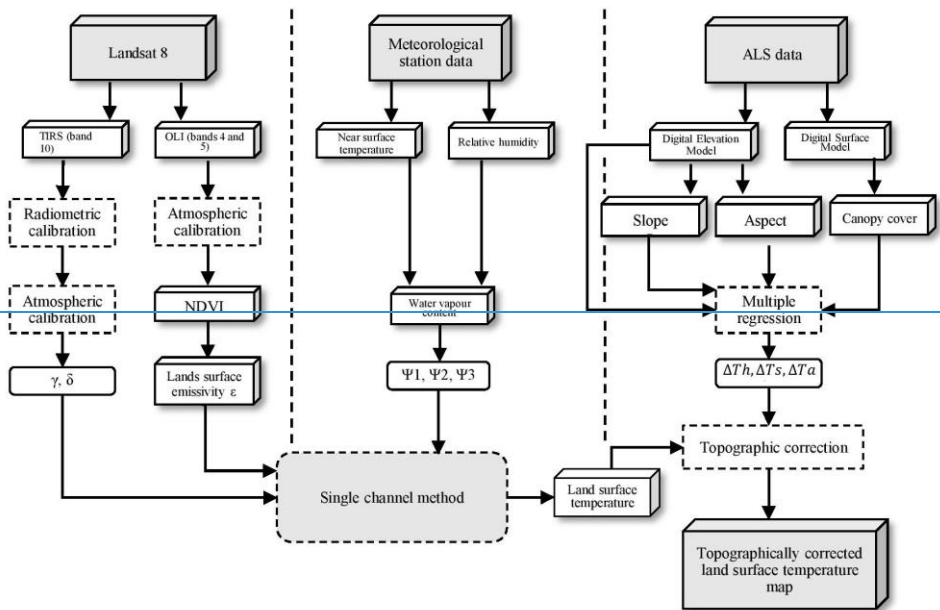
We conducted similar topographic correction with the Landsat image as with microclimate sensors to exclude the effect of topography on LST. Topographic variables (elevation, slope and aspect), ~~CC, and their interaction terms were included as independent factors and LST as the dependent factor in four multiple regression models (Table 2), and LST were included in a multiple regression model.~~ We classified aspect to nine classes indicating eight cardinal directions (south, south-west, west, north-west, north, north-east, east, south-east), and flat surface. The classes were treated as dummy variables due to their categorical nature. ~~We also classified elevation to three classes: below 1000 m, 1000–1500 m, and above 1500 m. We used the LST at elevation of 880 m, slope of 0 ° and aspect class north as reference. Following Wanderley et al. (2019), we calculated the topographically corrected LST with Eq. (6):~~

$$T' = T - \Delta T_h - \Delta T_s - \Delta T_a \quad (6)$$

~~Where  $T'$  = topographically corrected LST,  $T$  = raw LST,  $\Delta T_h$  = difference of  $T$  to the reference LST at elevation of 880 m,  $\Delta T_s$  = difference of  $T$  to the reference LST at slope of 0 °,  $\Delta T_a$  = difference of  $T$  to the reference LST in the aspect class “north”. We used linear regression to study how much CC percentage and topographic variables affected microclimate and LST. In total, we estimated four different models for LST (Table 2).~~

Model	Predictors
1	DEM, CC, slope, aspect (south, south-west, west, north-west, north, north-east, east, south-east)
2	DEM, CC, slope, aspect (south, south-west, west, north-west, north, north-east, east, south-east) elevation zones (<1000 m, 1000–1500 m, >1500 m), elevation zones * CC
3	DEM, CC, slope, aspect (south, south-west, west, north-west, north, north-east, east, south-east), DEM * CC
4	DEM, CC, slope, aspect (south, south-west, west, north-west, north, north-east, east, south-east), <a href="#">slope</a> <a href="#">* aspect classes</a> , elevation zones (<1000 m, 1000–1500 m, >1500 m), elevation zones * <a href="#">CC</a> , <a href="#">aspect</a> <a href="#">classes</a> * <a href="#">CC</a>

232 **Table 2:** Topographic and canopy cover (CC) predictors included in the four multiple regression models used in the  
 233 analysis of Landsat 8 [L](#)and surface temperature.



234  
 235 **Figure 2:** The workflow of Landsat 8 processing following the methodology by Ndossi and Avdan (2016), and  
 236 topographic correction.

237

### 238 3. Results

#### 239 3.1 Canopy cover and microclimate

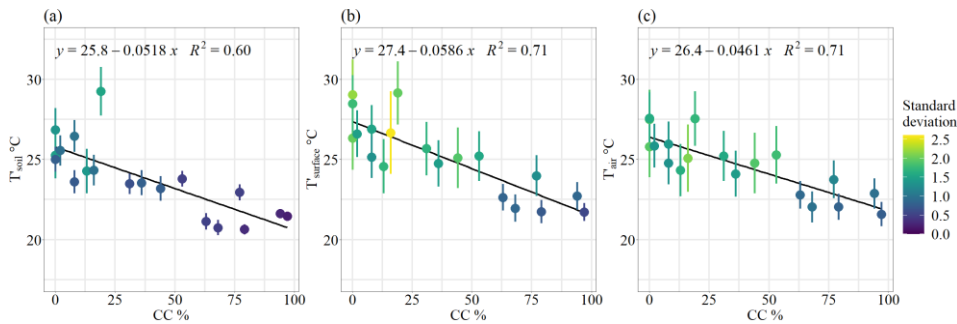
##### 240 3.1.1 Mean, maximum and minimum temperatures Temporal variation

241 Topographically corrected mean temperatures ( $T'$ ) had significant negative correlation with CC at all the measurement  
242 heights ( $T'_{\text{surface}}$  and  $T'_{\text{air}}$   $r = -0.84$ ,  $T'_{\text{soil}}$   $r = -0.78$ ). Based on the linear regression, an increase from 0 % to 100 % CC  
243 decreased  $T'_{\text{soil}}$  by 5.2 °C ( $R^2 = 0.6$ ),  $T'_{\text{surface}}$  by 5.9 °C ( $R^2 = 0.71$ ) and  $T'_{\text{air}}$  by 4.6 °C ( $R^2 = 0.71$ ) (Fig. 2). The average  
244 effect on combined  $T'_{\text{soil}}$ ,  $T'_{\text{surface}}$  and  $T'_{\text{air}}$  was 5.2 °C ( $R^2 = 0.68$ ).  $T'_{\text{surface}}$  and  $T'_{\text{air}}$  were in general higher than  $T'_{\text{soil}}$ .  
245 CC also affected variability of mean temperatures: SD of temperatures decreased by approximately 0.1 per 10 CC%  
246 increase at all measurement heights (Fig. 2). In  $T'_{\text{air}}$ , the relationship was not as evident as in  $T'_{\text{soil}}$  and  $T'_{\text{surface}}$ : SD  
247 decreased distinctly first when CC% was higher than 60 %.

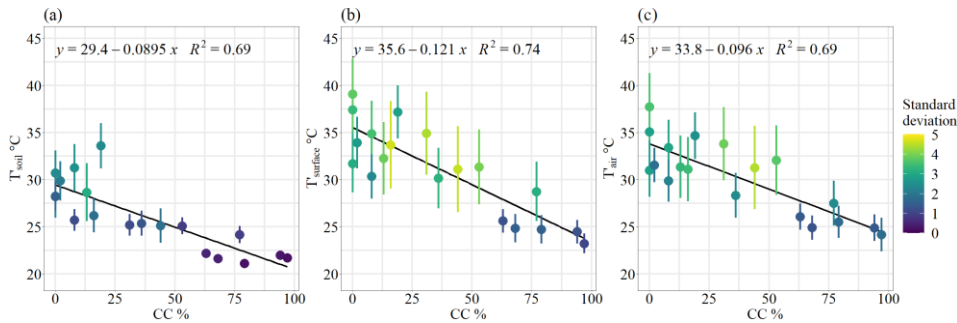
248 CC had a strong effect on maximum temperatures at all measurement heights,  $T'_{\text{surface}}$  being affected the most. High CC  
249 sites experienced the lowest  $T'_{\text{surface}}$  and  $T'_{\text{air}}$  maxima, while  $T'_{\text{surface}}$  and  $T'_{\text{air}}$  were the hottest in Maktau and sites with 0  
250 % CC. Here, topographically corrected average maximum temperatures ranged between 30 °C and 38.5 °C. Again,  $T'_{\text{surface}}$   
251 and  $T'_{\text{air}}$  were generally higher than  $T'_{\text{soil}}$ . The linear models showed that the increase from 0 % CC to 100 % CC decreased  
252 the maximum  $T'_{\text{soil}}$  by 9 °C ( $R^2 = 0.69$ ),  $T'_{\text{surface}}$  by 12.1 °C ( $R^2 = 0.74$ ) and  $T'_{\text{air}}$  by 9.6 °C ( $R^2 = 0.69$ ) (Fig. 3). On average,  
253 the difference was 10.2 °C. Similarly to mean temperatures, SD of maximum temperatures decreased with increasing CC:  
254  $T'_{\text{soil}}$  showed a more gradual decrease than  $T'_{\text{soil}}$  and  $T'_{\text{surface}}$ , where SD decreased substantially only in high CC sites (Fig.  
255 3). The SD of maximum temperatures were higher than in mean temperatures.

256 Based on the regression coefficients, which indicate the magnitude of the influence of CC on temperature, the cooling  
257 effect of CC was stronger on maximum temperatures than mean. Additionally, whereas CC affected mean  $T'_{\text{soil}}$  more than  
258 mean  $T'_{\text{air}}$ , in maximum temperatures the situation was the opposite, and  $T'_{\text{air}}$  was more affected by CC than  $T'_{\text{soil}}$  (Fig. 2  
259 and Fig. 3). Figure 3 presents the daily variation in topographically corrected daytime mean temperatures ( $T'$ ). The effect  
260 of CC was evident at all three measurement heights (soil, surface, air): mean temperatures were lower in high CC sites  
261 than in open areas, yet some low CC sites exhibited relatively low temperatures. On the hottest day of the study period  
262 (July 2), temperature differences between the hottest (Maktau, 19% CC) and coolest (Ngangao 1, 94% CC) sites were  
263 11.0 °C in  $T'_{\text{soil}}$ , 11.3 °C in  $T'_{\text{surface}}$  and 9.8 °C in  $T'_{\text{air}}$ . Even during colder days, temperatures were approximately 6.5 °C  
264 lower in sites with dense canopies than in open land.

265 CC affected also temperature variability: SD of temperature decreased by approximately 0.1 per 10 CC% increase at all  
 266 measurement heights. Especially  $T'_{soil}$  in the sites with high CC remained relatively stable from day to day, showing little  
 267 fluctuation even during the hot day streaks: differences remained even less than 1 °C between hottest and coolest days.  
 268 When comparing the three measurement heights, the coldest mean temperatures were measured in  $T'_{air}$  and the hottest in  
 269  $T'_{surface}$ . Temperatures varied more in  $T'_{surface}$  (SD = 3.0) and  $T'_{air}$  (SD = 2.7) than in  $T'_{soil}$  (SD = 2.3).

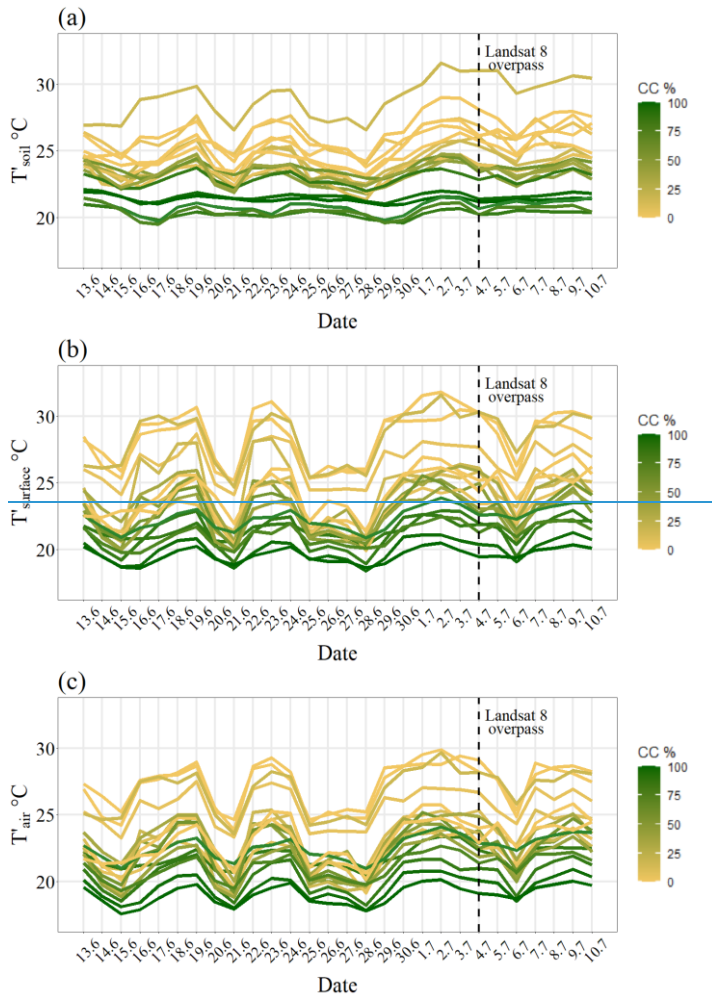


270  
 271 **Figure 2:** Scatterplots of topographically corrected daytime mean temperatures ( $T'$ ) and standard deviation against  
 272 canopy cover (CC) percentage, with regression line. a) Soil temperature. b) Surface temperature. c) Air temperature.



273  
 274 **Figure 3:** Scatterplots of topographically corrected daytime maximum temperatures ( $T'$ ) and standard deviation against  
 275 canopy cover (CC) percentage, with regression line. a) Soil temperature. b) Surface temperature. c) Air temperature.

276  
 277 Minimum temperatures showed no explicit relationship with CC, and sites with similar CC had high temperature  
 278 variability.  $R^2$  were low ( $< 0.2$ ) at all measurement heights, and correlations between temperatures and CC were  
 279 insignificant. All results from the regression analyses are summarized in Table 3.



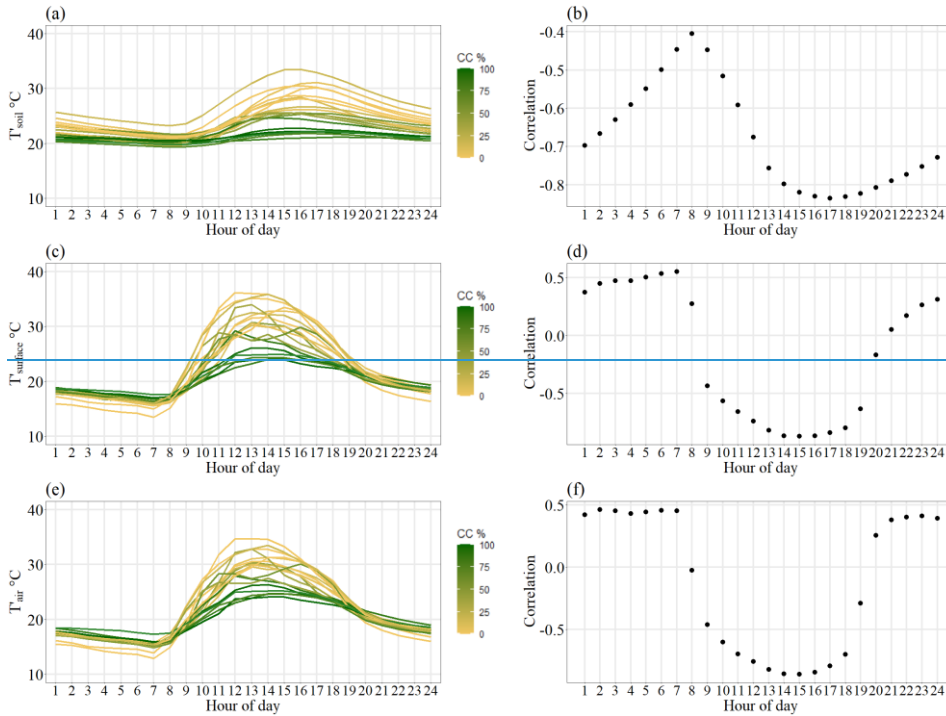
280

281 **Figure 3:** Daily variation in topographically corrected daytime (6.30–18.30) mean temperatures ( $T'$ )  
 282 between June 13 and July 10, 2019. Line color indicates canopy cover (CC) percentage. Dashed line  
 283 represents the overpass date of Landsat 8, July 4, 2019. a) Soil temperature. b) Surface temperature.  
 284 c) Air temperature.

285 Figure 4 shows the intra-daily temperature variability based on study period means.  $T'_{soil}$  were more stable than  $T'_{surface}$   
 286 and  $T'_{air}$  that showed higher peaks and drops. In the morning, temperatures at all measurement heights started to rise  
 287 rapidly between 6:00 and 8:00. Changes in  $T'_{soil}$  seemed to lag a couple of hours behind  $T'_{surface}$  and  $T'_{air}$ : they reached

288 highest readings between 11:00 and 15:00, while  $T'_{soil}$  peaked between 15:00 and 17:00. Further, after peaking,  
 289 temperatures decreased before stabilizing between 19:00 and 20:00 in  $T'_{surface}$  and  $T'_{air}$ , while  $T'_{soil}$  decreased slower.  $T'_{soil}$   
 290 remained warmer during the night than the other two.

291 Figure 4 also describes the correlation between CC% and temperatures. The impact of CC was the lowest in the morning,  
 292 when the temperatures also reached their minima. The strongest correlation ( $r < -0.8$ ) occurred during afternoon at all  
 293 measurement heights.  $T'_{soil}$  correlated negatively with CC% throughout the day, in contrast to  $T'_{surface}$  and  $T'_{air}$ , where  
 294 correlations were positive during the night.



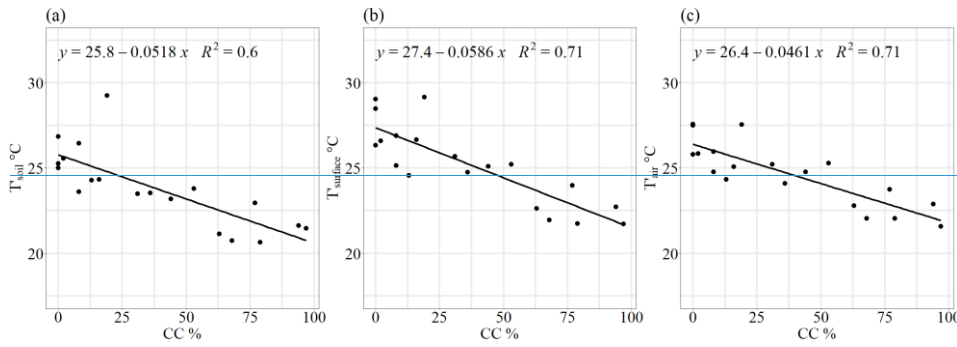
295  
 296 *Figure 4: Topographically corrected diurnal mean temperatures ( $T'$ ) (left) and the correlation between  $T'$  and canopy*  
 297 *cover (CC) percentage (right) between June 13 and July 10, 2019. Hour refers to ordinal number of hour, e.g. 1 means*  
 298 *00:00–01:00. Line color indicates CC percentage. a–b) Soil temperature. c–d) Surface temperature. e–f) Air temperature.*

299

### 300 3.1.2 Mean, maximum and minimum temperatures

301 Mean temperatures had significant negative correlation with CC at all the measurement heights ( $T_{\text{surface}}^{\text{d}}$  and  $T_{\text{air}}^{\text{d}}$   $r = -$   
 302  $0.84$ ,  $T_{\text{soil}}^{\text{d}}$   $r = -0.78$ ). Based on the linear regression, an increase from 0% to 100% CC decreased  $T_{\text{soil}}^{\text{d}}$  by  $5.2^{\circ}\text{C}$  ( $R^2 =$   
 303  $0.6$ ),  $T_{\text{surface}}^{\text{d}}$  by  $5.9^{\circ}\text{C}$  ( $R^2 = 0.71$ ) and  $T_{\text{air}}^{\text{d}}$  by  $4.6^{\circ}\text{C}$  ( $R^2 = 0.71$ ) (Fig. 5). The average effect on combined  $T_{\text{soil}}^{\text{d}}$ ,  $T_{\text{surface}}^{\text{d}}$   
 304 and  $T_{\text{air}}^{\text{d}}$  was  $5.7^{\circ}\text{C}$  ( $R^2 = 0.65$ ).  $T_{\text{surface}}^{\text{d}}$  and  $T_{\text{air}}^{\text{d}}$  were in general higher than  $T_{\text{soil}}^{\text{d}}$ , which was a case also with temperature  
 305 maxima.

306 CC had a strong effect on maximum temperatures at all measurement heights,  $T_{\text{surface}}^{\text{m}}$  being affected the most. High CC  
 307 sites experienced the lowest  $T_{\text{surface}}^{\text{m}}$  and  $T_{\text{air}}^{\text{m}}$  maxima, while  $T_{\text{surface}}^{\text{m}}$  and  $T_{\text{air}}^{\text{m}}$  were the hottest in Maktau and sites with  
 308 zero % CC. Here, average maximum temperatures ranged between  $30^{\circ}\text{C}$  and  $38.5^{\circ}\text{C}$ . The linear models showed that the  
 309 increase from zero % CC to 100% CC decreased the maximum  $T_{\text{soil}}^{\text{m}}$  by  $9^{\circ}\text{C}$  ( $R^2 = 0.69$ ),  $T_{\text{surface}}^{\text{m}}$  by  $12.1^{\circ}\text{C}$  ( $R^2 = 0.74$ )  
 310 and  $T_{\text{air}}^{\text{m}}$  by  $9.6^{\circ}\text{C}$  ( $R^2 = 0.69$ ) (Table 3). On average, the difference was  $10.2^{\circ}\text{C}$ . Based on the model coefficients, which  
 311 indicate the magnitude of the influence of CC on temperature, the cooling effect of CC was stronger on maximum  $T_{\text{soil}}^{\text{m}}$   
 312 and  $T_{\text{surface}}^{\text{m}}$  than mean, while CC affected  $T_{\text{air}}^{\text{m}}$  mean more than maximum.



313  
 314 **Figure 5:** Scatterplots of topographically corrected daytime mean temperatures ( $T^{\text{d}}$ ) against canopy  
 315 cover (CC) percentage, with regression line. a) Soil temperature. b) Surface temperature. c) Air  
 316 temperature.

317  
 318 Minimum temperatures showed no explicit relationship with CC, and sites with similar CC% had high temperature  
 319 variability.  $R^2$  were low ( $< 0.2$ ) at all measurement heights, and correlations between temperatures and CC were  
 320 insignificant.

321



	Measur ement height	Max (C°)	Site, CC %	Min (C°)	Site, CC %	Coef	R <sup>2</sup>	r	p-value
Mean	T <sub>soil</sub>	29.3	Maktau, 19 %	20.6	Bura river, 79 %	-0.052	0.604	-0.777	<0.001*
	T <sub>surface</sub>	29.2	Maktau, 19 %	21.7	Chawia, 97 %	-0.059	0.711	-0.843	<0.001*
	T <sub>air</sub>	27.6	Sarova 2, 0 %	21.6	Chawia, 97 %	-0.046	0.710	-0.842	<0.001*
Maximum	T <sub>soil</sub>	33.3	Maktau, 19 %	20.8	Bura river, 79 %	-0.09	0.693	-0.832	<0.001*
	T <sub>surface</sub>	38.8	Sarova 2, 0 %	22.9	Chawia, 97 %	-0.121	0.742	-0.862	<0.001*
	T <sub>air</sub>	37.4	Sarova 2, 0 %	23.8	Chawia, 97 %	-0.1	0.686	-0.828	<0.001*
Minimum	T <sub>soil</sub>	23.0	Maktau, 19 %	19.2	Bura, 68 %	-0.003	0.083	-0.289	0.231
	T <sub>surface</sub>	19.5	Chawia, 97 %	12.9	Sarova 2, 0 %	-0.024	0.189	0.435	0.063
	T <sub>air</sub>	19.3	Ngangao 2, 77 %	12.3	Sarova 2, 0 %	-0.023	0.149	0.386	0.102

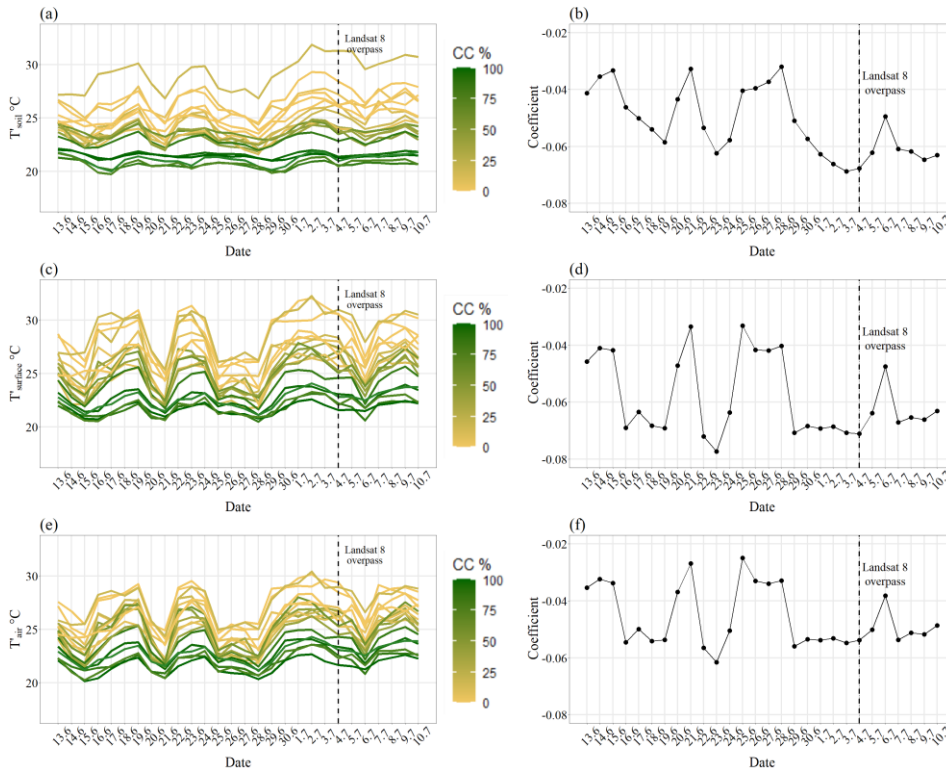
322 **Table 3.** Topographically corrected temperature (T') statistics for the soil, surface and air. Temperatures in the maximum  
323 and minimum columns refer to the highest and lowest mean, maximum and minimum temperatures. Site refers to where  
324 the highest and lowest temperatures were measured and their respective canopy cover (CC) percentage. \* indicates  
325 statistical significance.

### 326 3.1.2 Temporal variation

327 [Figure 4 presents the daily variation in topographically corrected daytime mean temperatures. The effect of CC was](#)  
328 [evident at all three measurement heights: mean temperatures were lower in high CC sites than in open areas, yet some](#)  
329 [low CC sites exhibited relatively low temperatures. For example, on July 2, which was one of the hottest days of the study](#)  
330 [period, temperature differences between the hottest \(Maktau, 19 % CC\) and coolest \(Ngangao 1, 94 % CC\) sites were](#)  
331 [11.0 °C in T<sub>soil</sub>, 11.3 °C in T<sub>surface</sub> and 9.8 °C in T<sub>air</sub>. Even during the coldest days, temperatures were lower in sites with](#)  
332 [dense canopies than in open land. Especially T<sub>soil</sub> in the sites with high CC remained relatively stable from day to day,](#)  
333 [showing little fluctuation even during the hot day streaks: differences in mean temperatures remained even less than 1 °C](#)  
334 [between hottest and coolest days.](#)

335 [The cooling effect of CC varied throughout the study period: on hot days, the cooling effect \(described by CC's regression](#)  
336 [coefficient in Fig. 4\) increased, while on cooler days, the cooling effect decreased. The strongest cooling took place in](#)

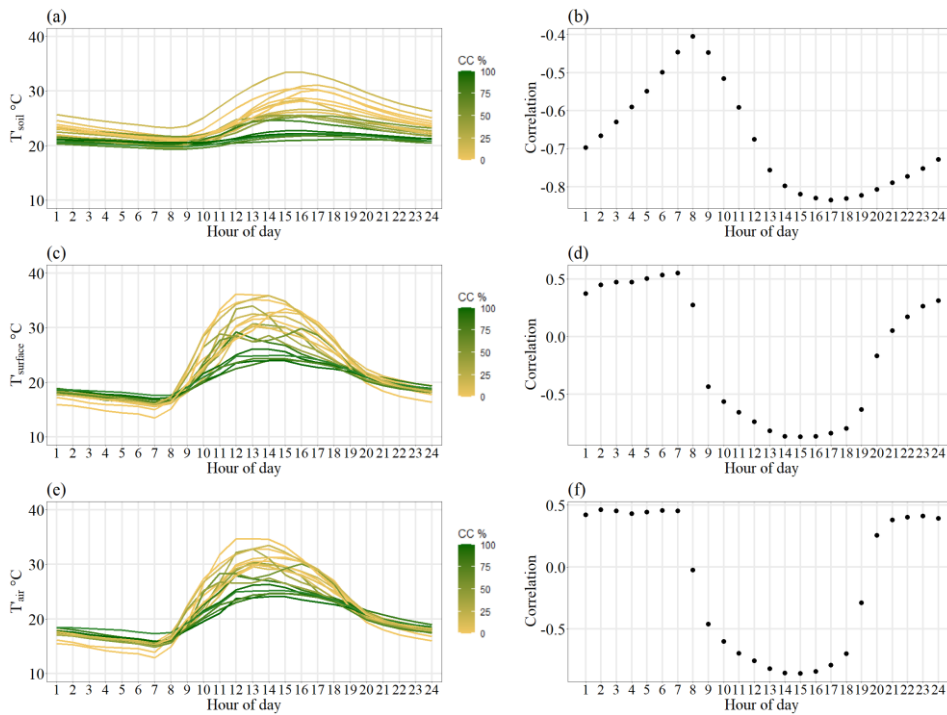
337  $T_{\text{surface}}$  on June 23, when CC's cooling effect was 7.6 °C.  $T_{\text{surface}}$  had overall the highest cooling effect (3.3 °C–7.6 °C)  
 338 and  $T_{\text{air}}$  the weakest (2.6 °C–6 °C). In  $T_{\text{soil}}$ , the cooling effect was 3.2 °C–6.9 °C (Fig. 4).



339  
 340 **Figure 4:** Daily variation in topographically corrected daytime (6.30–18.30) mean temperatures ( $T$ ) between June 13  
 341 and July 10, 2019 (left), and cooling effect of canopy cover (described by regression coefficient) (right). Line color  
 342 indicates canopy cover (CC) percentage. Dashed line represents the overpass date of Landsat 8, July 4, 2019. a–b) Soil  
 343 temperature. c–d) Surface temperature. e–f) Air temperature.

344 Figure 5 shows the intra-daily temperature variability based on study period means.  $T_{\text{soil}}$  were more stable than  $T_{\text{surface}}$   
 345 and  $T_{\text{air}}$  that showed higher peaks and drops. In the morning, temperatures at all measurement heights started to rise  
 346 rapidly between 6:00 and 8:00. Changes in  $T_{\text{soil}}$  seemed to lag a couple of hours behind  $T_{\text{surface}}$  and  $T_{\text{air}}$ : they reached  
 347 highest readings between 11:00 and 15:00, while  $T_{\text{soil}}$  peaked between 15:00 and 17:00. Further, after peaking,  
 348 temperatures decreased before stabilizing between 19:00 and 20:00 in  $T_{\text{surface}}$  and  $T_{\text{air}}$ , while  $T_{\text{soil}}$  decreased slower.  $T_{\text{soil}}$   
 349 remained warmer during the night than the other two measurement heights.

350 Figure 5 also describes the correlation between CC and temperatures. The impact of CC was the lowest in the morning,  
 351 when the temperatures also reached their minima. The strongest correlation ( $r < -0.8$ ) occurred during afternoon at all  
 352 measurement heights.  $T_{soil}$  correlated negatively with CC throughout the day, in contrast to  $T_{surface}$  and  $T_{air}$ , where  
 353 correlations were positive during the night.



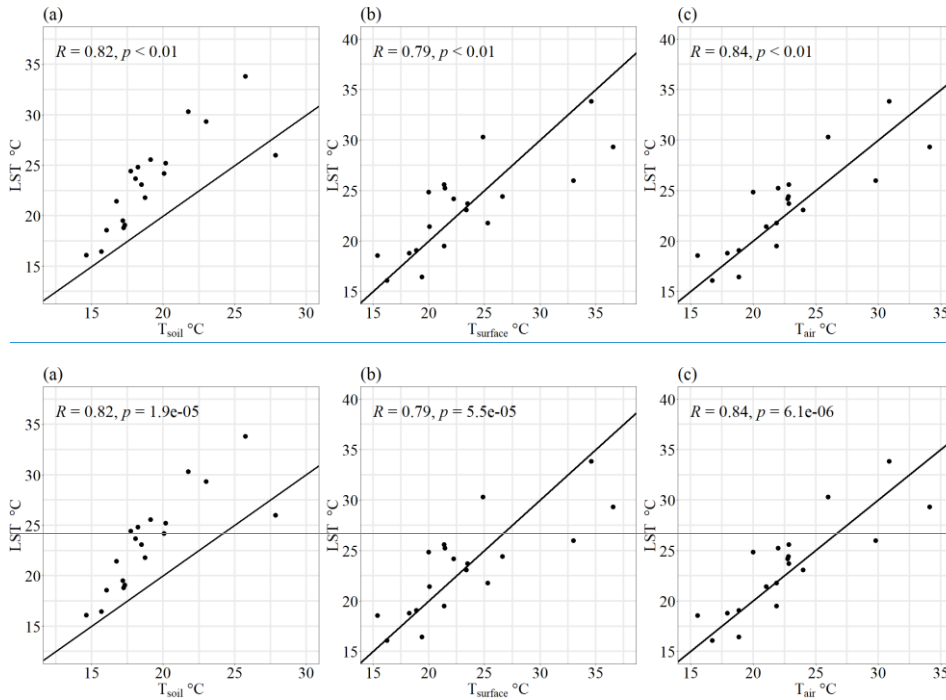
354  
 355 **Figure 5:** Topographically corrected diurnal mean temperatures ( $T'$ ) (left) and the correlation between  $T'$  and canopy  
 356 cover (CC) percentage (right) between June 13 and July 10, 2019. Hour refers to ordinal number of hour, e.g. 1 means  
 357 00:00–01:00. Line color indicates CC percentage. a–b) Soil temperature. c–d) Surface temperature. e–f) Air temperature.

358  
 359 **3.2 Landsat 8 LST and surface temperature**

360 **3.2.1 Land surface temperature compared with temperatures measured in the field**

361 LST and raw field temperatures ( $T$ ) at the time of satellite overpass showed statistically significant correlation ( $r = 0.82$ ,  
 362 0.79 and 0.84 at  $T_{soil}$ ,  $T_{surface}$  and  $T_{air}$ , respectively) (Fig. 66). At 18 sites out of 19, LST was higher than  $T_{soil}$ , whereas

363 between LST and  $T_{\text{surface}}$  or  $T_{\text{air}}$  there was no consistent difference. Mean differences were 4.1 °C ( $T_{\text{soil}}$ ), -0.03 °C ( $T_{\text{surface}}$ )  
 364 and 0.57 °C ( $T_{\text{air}}$ ). The  $T_{\text{soil}}$  difference was statistically significant with 95 % confidence, while  $T_{\text{surface}}$  and  $T_{\text{air}}$  not.



366  
 367 **Figure 66:** Landsat 8 land surface temperature (LST) compared with raw field temperatures (T) at the time of satellite  
 368 overpass (10:30) on July 4, 2019. a) LST and soil temperature. b) LST and surface temperature. c) LST and air  
 369 temperature.

370  
 371 **3.2.2 Impact of canopy cover and topography on land surface temperature**

372 Topographic variables elevation, slope and aspect had all a significant effect on LST. In all four models, the elevational  
 373 lapse rates varied from 11 °C km<sup>-1</sup> to 15 °C km<sup>-1</sup>. Aspect, in turn, had a varying impact depending on the model, but the  
 374 general trend was that south, south-west and west had the highest cooling, as was expected at the time of the day. The  
 375 effect of slope decreased as the models became more complex, and the joint impacts of slope and aspect in Model 4 were  
 376 greater than the effects of slope or aspect alone. The results of all four models can be found in Appendix B.

377 All the variables in Model 1 showed statistical significance ( $R^2 = 0.74$ ). Based on the regression analysis, generally the  
 378 increase from ~~zero~~ 0% CC to 100% CC decreased LST with 5 °C (Table 4). After the exclusion of other variables except  
 379 CC, correlation between LST and CC was -0.37 ( $p < 0.001$ ) and  $R^2 = 0.14$ . ~~Topographic correction based on Model 1~~  
 380 ~~improved the correlation coefficient to -0.42 and  $R^2$  to 0.18.~~

381 In Model 2, three elevation zones (below 1000 m, 1000–1500 m, above 1500 m) were added to the model. This increased  
 382 the  $R^2$  to 0.77, demonstrating a notable difference in the cooling effect of CC depending on elevation zone. At the  
 383 elevations below 1000 m, the cooling effect of CC when moving from 0zero % CC to 100% CC was -6.86 °C, between  
 384 1000–1500 m the effect was -3.72 °C, and above 1500 m the effect was -42.8 °C (Table 4). Roughly, the cooling impact  
 385 of CC ~~above 1000 m was about a half in the hills compared to the effect in the lowlands~~ decreased to almost half of the  
 386 ~~impact in the lowlands.~~

387 In Model 3, the interaction term of CC and elevation zones was replaced with interaction term of CC and the continuous  
 388 variable elevation from the DEM. This produced  $R^2 = 0.74$ . The coefficient for the interaction term was 0.00005,  
 389 indicating that ~~an~~ increase of 1000 m in elevation decreased the cooling effect of CC by 0.05 °C (Table 4). The model  
 390 performed poorer compared to Model 2.

391 Model 4 was built up on Model 2 by adding interaction terms between ~~slope and aspect classes and CC~~ (Table 4). ~~Model~~  
 392 ~~4 performed best of the four ( $R^2 = 0.77$ ), but the difference was not large compared to Model 2. The cooling effect of CC~~  
 393 ~~in the lowlands was 6.8 °C, the same as in Model 2. In the elevation zone 1000–1500 m the cooling effect was 3.7 °C and~~  
 394 ~~above 1500 m it was 3 °C. The cooling effect of CC in 1000–1500 m had the same magnitude as in Model 2, and it~~  
 395 ~~decreased by further 0.7 °C in elevations above 1500 m. According to the results from Model 4, the magnitude of aspect's~~  
 396 ~~influence on the cooling effect of CC was mostly insignificantly small, except in the cases of north-east, east and south-~~  
 397 ~~east, where the coefficients decreased by roughly 0.01 °C. Model 4 performed best of the four ( $R^2 = 0.77$ ).~~

398 In summary, including either of the elevation factors (DEM or elevation zones) in the model showed that elevation  
 399 affected CC's cooling effect significantly, having ~~almost~~ two times higher impact in the lowlands compared to the hills.  
 400 The dependence of CC's impact on elevation is demonstrated in Fig. 77 using eight elevation classes. CC's ~~regression~~  
 401 coefficients decreased with increasing elevation after 1000 m, yet increased again between 1200–1400 m to roughly the  
 402 same as in the lowlands. The effect was the smallest in elevations above 1800 m.

Predictor	Model	Coef	Std. Error	T-Value	P-Value
Constant	1	44.79	0.013	3324.0	<0.001*

Formatted: Graduteksti

Formatted: Graduteksti, Left

	2	44.24	0.019	2300.9	<0.001*
	3	46.71	0.018	2580.3	<0.001*
	4	44.38	0.021	2142.5	<0.001*
	1	-0.013	0.000	-1241.4	<0.001*
Elevation	2	-0.011	0.000	-577.2	<0.001*
	3	-0.015	0.000	-954.6	<0.001*
	4	-0.011	0.000	-579.3	<0.001*
	1	-4.061	0.018	-220.0	<0.001*
Slope	2	-3.806	0.018	-214.9	<0.001*
	3	-3.723	0.018	-202.3	<0.001*
	4	-3.781	0.018	-212.6	<0.001*
	1	-0.050	0.000	-419.0	<0.001*
Canopy cover	2	-0.068	0.000	-449.1	<0.001*
	3	-0.109	0.000	-274.7	<0.001*
	4	-0.073	0.000	-208.0	<0.001*
	1	0.177	0.011	16.0	<0.001*
NE	2	0.084	0.010	8.1	<0.001*
	3	0.157	0.011	14.3	<0.001*
	4	-0.215	-0.015	-14.0	<0.001*
	1	-0.030	0.010	-29.0	<0.001*
E	2	-0.428	0.010	-44.6	<0.001*
	3	-0.352	0.010	-34.7	<0.001*
	4	-0.766	0.014	-55.2	<0.001*

Formatted: Graduteksti, Left

Formatted: Graduteksti, Left

Formatted: Graduteksti, Left

Formatted: Graduteksti, Left

Formatted: Graduteksti, Left

SE	1	-1.447	0.010	-140.0	<0.001*
	2	-1.509	0.010	-155.6	<0.001*
	3	-1.529	0.010	-149.3	<0.001*
	4	-1.733	0.014	-127.3	<0.001*
<hr/>					
S	1	-2.095	0.011	-189.4	<0.001*
	2	-2.132	0.010	-205.2	<0.001*
	3	-2.186	0.011	-199.4	<0.001*
	4	-2.166	0.014	-153.3	<0.001*
<hr/>					
SW	1	-2.441	0.011	-230.0	<0.001*
	2	-2.554	0.010	-256.0	<0.001*
	3	-2.527	0.011	-240.1	<0.001*
	4	-2.538	0.014	-185.9	<0.001*
<hr/>					
W	1	-2.293	0.010	-219.5	<0.001*
	2	-2.254	0.010	-229.9	<0.001*
	3	-2.332	0.010	-225.5	<0.001*
	4	-2.195	0.014	-159.0	<0.001*
<hr/>					
NW	1	-1.380	0.011	-126.8	<0.001*
	2	-1.205	0.010	-117.9	<0.001*
	3	-1.379	0.012	-127.9	<0.001*
	4	-1.196	0.015	-81.9	<0.001*
<hr/>					
1000-1500-m	1	∓	∓	∓	∓
	2	-2.667	0.008	-346.9	<0.001*
	3	∓	∓	∓	∓

Formatted: Graduteksti, Left

Formatted: Graduteksti, Left

Formatted: Graduteksti, Left

Formatted: Graduteksti, Left

Formatted: Graduteksti, Left

Formatted: Graduteksti

	4	-2.678	0.008	-348.5	<0.001*
	1	∞	∞	∞	∞
>1500 m	2	-2.030	0.018	-111.2	<0.001*
	3	∞	∞	∞	∞
	4	-2.006	0.018	-110.0	<0.001*
	1	∞	∞	∞	∞
Canopy cover: 1000-1500 m	2	0.031	0.000	149.7	<0.001*
	3	∞	∞	∞	∞
	4	0.032	0.000	153.5	<0.001*
	1	∞	∞	∞	∞
Canopy cover: >1500m	2	0.028	0.000	120.7	<0.001*
	3	∞	∞	∞	∞
	4	0.038	0.000	121.6	<0.001*
	1	∞	∞	∞	∞
Elevation: canopy cover	2	∞	∞	∞	∞
	3	0.00005	0.000	156.3	<0.001*
	4	∞	∞	∞	∞
	1	∞	∞	∞	∞
Canopy cover: NE	2	∞	∞	∞	∞
	3	∞	∞	∞	∞
	4	0.011	0.000	25.6	<0.001*
	1	∞	∞	∞	∞
Canopy cover: E	2	∞	∞	∞	∞

Formatted: Graduteksti

Formatted: Graduteksti

Formatted: Graduteksti

Formatted: Graduteksti

Formatted: Graduteksti

Formatted: Graduteksti



	3	±	±	±	±
	4	0.013	0.000	32.6	<0.001*
<hr/>					
Canopy cover: SE	1	±	±	±	±
	2	±	±	±	±
	3	±	±	±	±
	4	0.010	0.000	24.0	<0.001*
<hr/>					
Canopy cover: S	1	±	±	±	±
	2	±	±	±	±
	3	±	±	±	±
	4	-0.000	0.000	-0.2	0.8
<hr/>					
Canopy cover: SW	1	±	±	±	±
	2	±	±	±	±
	3	±	±	±	±
	4	-0.003	0.000	-8.0	<0.001*
<hr/>					
Canopy cover: W	1	±	±	±	±
	2	±	±	±	±
	3	±	±	±	±
	4	-0.003	0.000	-7.8	<0.001*
<hr/>					
Canopy cover: NW	1	±	±	±	±
	2	±	±	±	±
	3	±	±	±	±
	4	-0.000	0.000	-1.2	0.25

Formatted: Graduteksti

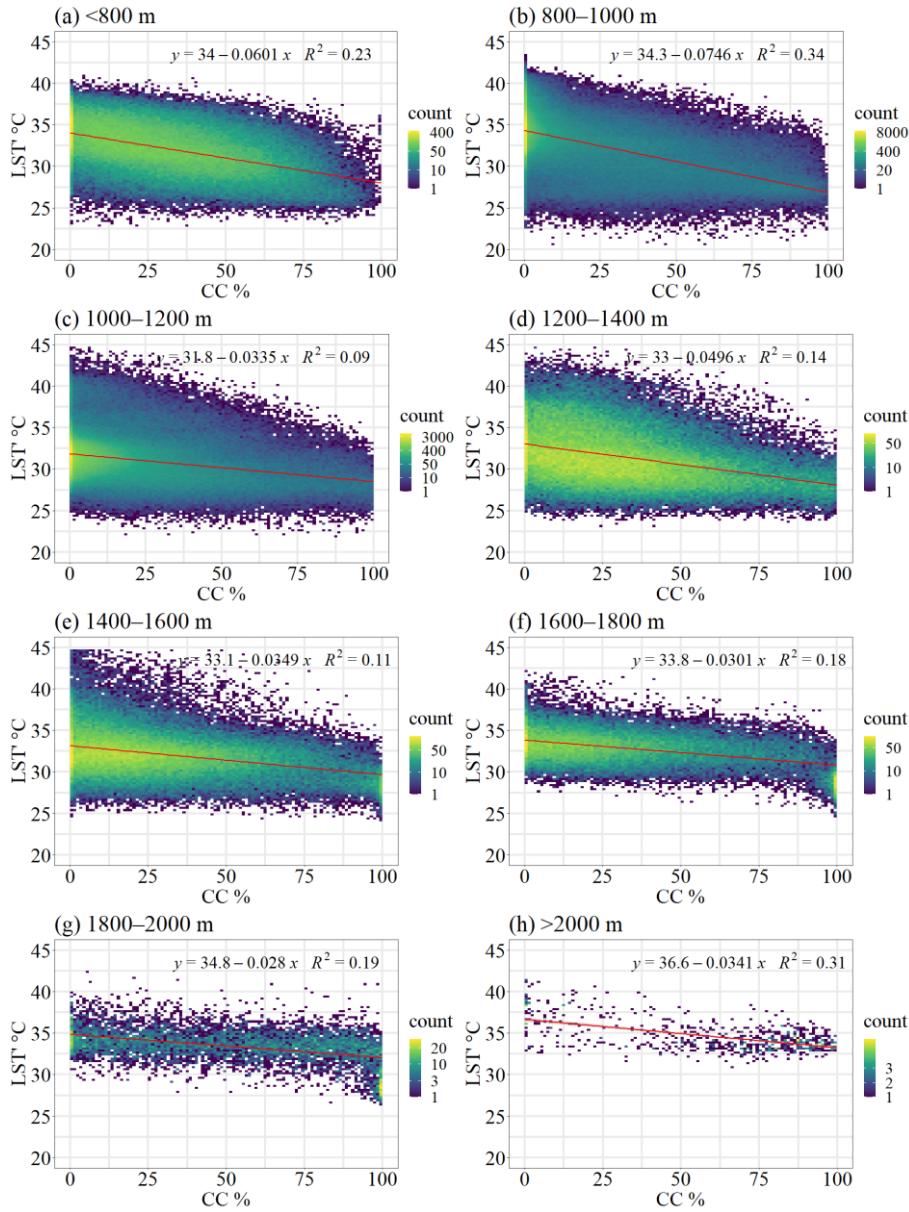
Formatted: Graduteksti

Formatted: Graduteksti

Formatted: Graduteksti

Formatted: Graduteksti

404 **Table 4:** Summary of regression coefficients in the analysis of land surface temperature (LST) from the four models  
 405 tested. \* indicates statistical significance.



406

407 **Figure 77:** Density plots of topographically corrected land surface temperature (LST') and canopy cover (CC) percentage  
408 in eight elevation classes, with regression line. a) below 800 m. b) 800–1000 m. c) 1000–1200 m. d) 1200–1400 m. e)  
409 1400–1600 m. f) 1600–1800 m. g) 1800–2000 m. h) above 2000 m.

410

#### 411 4. Discussion

412 High CC decreased near-ground mean temperatures on average by 5.27 °C compared to open land, depending on  
413 measurement height. The difference was even greater in temperature maxima, which has been reported to be the case also  
414 by De Frenne et al. (2019) and Belsky et al. (1989). Temperature and CC had a linear relationship, pointing out that closed  
415 CC was not needed for a [sensible-substantial](#) cooling effect.

416 T<sub>surface</sub> was affected the most by CC. Despite the measurement height of T<sub>surface</sub> being only 13 cm below T<sub>air</sub>, the effect of  
417 CC was notably weaker in T<sub>air</sub>, which is in line with previous studies. For example, [Davis et al. \(2019\) report that the](#)  
418 [effect of CC was weaker at 2 m than at 10 cm height, while in De Frenne et al. \(2019\) temperature offset between forest](#)  
419 [and open land was the greatest close to the ground. In Belsky et al. \(1989\), soil temperature was the least affected by CC.](#)  
420 [Luyssaert et al. \(2014\) compared air temperature and LST and report that the temperature of the planetary boundary was](#)  
421 [less affected than LST by the removal of forest cover. Luyssaert et al. \(2014\) report that the temperature of the planetary](#)  
422 [boundary was less affected than LST by the removal of forest cover, while in De Frenne et al. \(2019\) temperature offset](#)  
423 [between forest and open land was the greatest close to the ground. In Belsky et al. \(1989\), soil temperature was the least](#)  
424 [affected by CC.](#)

425 ~~The prevalent temperatures~~Macroclimate affected the magnitude of the cooling: [based on the temporal data from the](#)  
426 [microclimate sensors, during the cooler days of overcast conditions, CC's cooling effect was smaller. Additionally, the](#)  
427 [temperature differences between low and high CC sites were smaller during these days. In the case of LST, elevation](#)  
428 [impacted the cooling effect; in elevations above 1000 m, the cooling effect decreased remarkably by approximately 50 %](#)  
429 [compared to that of the lowlands. It can be concluded that trees' importance in controlling temperatures increases in](#)  
430 [hotter environments.](#) ~~Moreover, based on the temporal data from the microclimate sensors, during the cooler days of~~  
431 ~~overcast conditions, CC's cooling effect was smaller. Additionally, the temperature differences between low and high CC~~  
432 ~~sites were smaller during these days. One likely reason behind the phenomenon is that plant evapotranspiration rates are~~  
433 ~~relative to the solar radiation and ambient temperatures (Allen et al. 1998). It can be concluded that trees' importance in~~  
434 ~~controlling temperatures increases in hotter environments.~~The [discovery finding](#) is meaningful, [since because](#) agricultural  
435 expansion on the cost of woody vegetation cover in the area is predicted to take place predominantly in the lowlands

436 (Erdogan et al. 2011; Maeda et al., 2010), where the temperatures are very high. Increasing tree cover on farmlands could  
437 thus be of considerable benefit in decreasing local temperatures.

438 [Our finding is in parallel to findings by Zeng et al. \(2021\), who reported an elevational effect of deforestation on](#)  
439 [temperatures in Albertine Rift Mountains: the warming effect of deforestation decreased with elevation and disappeared](#)  
440 [at elevations above 3000 m. This phenomenon resembles the latitude-dependent effect of forests on temperatures: in](#)  
441 [tropical areas, there is more cooling, while boreal forests cause more warming \(Lee et al., 2011; Li et al., 2015\). Plant](#)  
442 [evapotranspiration rates are relative to the solar radiation, ambient temperatures and water balance \(Geiger, 1980; Allen](#)  
443 [et al. 1998; Davis et al., 2019\), decreasing the demand for evapotranspiration in low temperatures caused by elevational](#)  
444 [lapse rate or cool weather conditions. During clear weather, canopies absorb and reflect most of the incoming solar](#)  
445 [radiation creating cooler conditions in the understory together with evapotranspiration, whereas cloud cover causes a total](#)  
446 [reduction in the incoming short-wave radiation \(Geiger, 1980; De Frenne et al., 2021\). Moreover, while the](#)  
447 [evapotranspirative cooling mostly offsets warming caused by canopy albedo, in high elevations the albedo effect stays](#)  
448 [constant and evapotranspiration decreases \(Zeng et al., 2021\).](#)

449 [The impact of CC on microclimate was different on different days, and is likely to vary during different times of the year](#)  
450 [\(Davis et al., 2019; De Frenne et al., 2021\). We expect this to be the case with LST as well.](#)~~[The impact of CC on](#)~~  
451 ~~[temperature is also most likely different on different days and different times of the year.](#)~~ For instance, Maeda and  
452 Hurskainen (2014) found that land cover's influence on LST in Mount Kilimanjaro varied seasonally and diurnally, and  
453 the effect was dependent on elevation. Our LST estimation [using the satellite image](#) was only a snapshot for July 4, 2019,  
454 ~~[from](#)~~ a sunny almost cloud-free day, and does not represent the year-round situation experiencing two rainy seasons,  
455 which are cloudy. In the hills, cloudy and misty conditions are experienced throughout the year (Helle, 2016; Räsänen et  
456 al., 2018). A time series comparing the cooling effect of CC over seasons and several years is an interesting future research  
457 topic, as the TOMST sensors remained in the 19 field plots. Interesting would also be to model the sunshine hours every  
458 day in the locations of the TOMST sensors using the hemispherical photography, in order to assess how many hours of  
459 the day the tree cover causes shadows [over](#) the sensor.

460 [Canopies control the thermal environments of forests to a high extent \(De Frenne et al., 2019; Davis et al., 2019\). The](#)  
461 ~~[thermal environments of forests are controlled by canopies to a high extent,](#)~~ which was reaffirmed in this study. Therefore,  
462 CC can mitigate large-scale macroclimate warming (De Frenne et al., 2019). An increase of 2 °C of the global temperature  
463 as a consequence of enhanced greenhouse effect can have detrimental impacts on the most vulnerable ecosystems (IPCC,  
464 2018). ~~[Since-Because](#)~~ the time span of local changes in temperatures due to LULCC is much shorter than in the global  
465 climate change, the regional and local consequences can be of even higher ~~[extent-magnitude](#)~~ (Potter et al., 2013; Chen et

466 al., 1999). Due to the debts of species' adaptation capabilities to climate warming (Zellweger et al., 2020), changes in the  
467 microclimate temperatures may be fatal for flora and fauna occupying narrow thermal niches. This may further impact  
468 biodiversity and consequently the crucial ecosystem services provided by forests that take place close to ground surface  
469 (Chen, et al. 1999; Zellweger et al., 2020).

470 Forest fragmentation decreases the ability of tropical forests to mitigate climate change (Ewers and Banks-Leite, 2013),  
471 but on regional scale even small forests have an impact on LST (Mildrexler et al., 2011). Our results [from the linear](#)  
472 [models](#) revealed that ~~trees on farms~~ TOF had the same effect on local temperatures as forests despite the smaller  
473 ~~scale~~ [magnitude](#), and could hence help in conserving ~~the~~ biodiversity. For instance, Mendenhall et al. (2016) found that in  
474 Costa Rica farm trees increased the number of tree and plant species. Most of the CC in Taita Hills comprises of TOF,  
475 occurring on farms and human settlement. Sites with agroforestry trees and moderate CC were already experiencing both  
476 lower mean and maximum temperatures than the open sites.

477 [The importance of TOF is receiving more attention \(Kuyah et al., 2019; Skole et al., 2021\), and in Taita Hills, Pellikka](#)  
478 [et al. \(2018\) reported an addition in carbon stocks since 2003. The Agriculture \(Farm Forestry\) Rules of 2009 requires](#)  
479 [that at least 10 % forest cover should be left or planted on farms. Based on our results, this 10 % CC makes a significant](#)  
480 [difference in temperatures \(-0.5 °C in mean and -1 °C in maximum temperatures; -0.5 °C in LST\). Soil and air](#)  
481 [temperatures have an impact to crop productivity, and furthermore, the fog deposit captured by trees brings more water](#)  
482 [to plants. In general, increasing temperatures make plant growth more efficient, but this is the case only as long as the](#)  
483 [increase occurs within the thermal limits of the plant's tolerance \(Muimba-Kankolongo, 2018\). As extreme heat and](#)  
484 [precipitation events are becoming more common with climate change \(MoALF, 2016; IPCC, 2018\), the negative effects](#)  
485 [of warming will become notable in sub-Saharan Africa. This further threatens the food security, and especially the most](#)  
486 [common crop, maize, which is one of the most vulnerable crops in terms of climate change in Africa \(Cairns et al., 2013;](#)  
487 [Adhikari et al., 2015\). Forests of Taita Hills contribute to the food security by capturing atmospheric moisture as fog](#)  
488 [deposit and storing the water providing water for farms in the foothills and lowlands \(Pellikka et al., 2013; Helle, 2016\).](#)  
489 [In addition to dew capture, agroforestry has shown to contribute to improved soil moisture \(Rhoades 1995; Siriri et al.](#)  
490 [2013\), hydraulic conductivity \(Nyamadzawo et al. 2003, 2007\) and water storage \(Makumba et al. 2006; Nyamadzawo](#)  
491 [et al. 2012\).](#)

492 The pressure on tropical forests in sub-Saharan Africa is caused by many reasons, fuelwood collection being significant  
493 (Abdelgalil, 2004, [Zschauer, 2012](#)), which could be mitigated by increasing the tree cover on farms (Unruh et al., 1993,  
494 [Iiyama et al., 2014; Chakravarty et al., 2019](#)). The results of this study further encourage to increase tree cover, ~~in~~  
495 ~~particular~~ [particularly](#) in the lowland farms, as a strong potential way to fight the negative effects of climate change.

496 Nevertheless, water is scarce especially in the lowland areas, and trees' vast need for water must be taken into account.

497 The phenomenon is paradoxical, ~~since because~~ trees improve the water cycle, in general, but are consumes high amounts  
498 of water (Ong et al., 2006). [Water balance also affects the temperature buffering capacity of trees \(Davis et al., 2019\)](#). In  
499 areas with water scarcity, the competition ~~for~~ water resources ~~with-between~~ crops, animals and people may be a limiting  
500 factor in the adoption of agroforestry practices. One solution in the hot lowlands is dew collection, but it would require a  
501 tree cover or other surfaces to capture the humidity. In Tuure et al. (2019), artificial surfaces produced at best 0.1 liter per  
502 day and 25 liters in a year water from morning dew.

503 This study was limited to a short time span and a small sample size in microclimate study sites, which makes it susceptible  
504 for uncertainties associated with temporal and spatial variability. Topographic correction was applied on the microclimate  
505 data and was calculated based on elevation only. The small amount of observations did not allow for calculating ~~on~~ the  
506 impact of the aspect, which is expected to exist based on the LST analysis. Due ~~to the topographic-accounting for the~~  
507 [effect of topography, both microclimate and LST estimates manipulation of the temperatures, they](#) did not represent the  
508 true values recorded, but made the temperatures comparable by CC.

509 ~~In terms of LST, as has been documented in several studies, spaceborne TIR remains an uncertain method for accurate~~  
510 [LST retrieval \(Simó et al., 2018; Li et al., 2013\)](#). After all, LST is an indirect measurement and the results of complicated  
511 [mathematical processing requiring knowledge of several components, where error in any of them causes inaccuracies in](#)  
512 [LST \(Simó et al., 2018\)](#). We calculated LST using the SC method by Jiménez-Muñoz and Sobrino (2004) due to the stray  
513 [light problem in Landsat 8 TIRS band 11. While using only one thermal channel for the estimation of LST exposes a high](#)  
514 [possibility of inaccuracy, band 10 is more suitable for the SC method than band 11 because of higher atmospheric](#)  
515 [transmissivity \(Jiménez-Muñoz et al., 2014\)](#). The main sources of error in SC are estimation of atmospheric water vapor  
516 [content and LSE. LSE is determinant in the correct LST retrieval, yet highly difficult to measure and prone to error. Water](#)  
517 [vapor, in turn, can be highly spatially variable, and should be retrieved preferably from satellite data rather than pointwise](#)  
518 [weather station data \(Ndossi and Avdan, 2016\)](#). Jiménez-Muñoz et al. (2014) report that water vapor content higher than  
519 [3 g cm<sup>-2</sup> causes unacceptable inaccuracy: in this study, the water vapor content was 1.7 g cm<sup>-2</sup>, which decreases the](#)  
520 [possible error. Wang et al. \(2019\) conclude that the SC is a valid method for Landsat 8 processing and produces results](#)  
521 [on accuracy high enough for most purposes: Ndossi and Avdan \(2016\) found that SC was the second best algorithm for](#)  
522 [the retrieval of Landsat 8 LST. SC has been applied successfully also by for example He et al. \(2019\), as has been](#)  
523 [documented in several studies, spaceborne TIR remains an uncertain method for accurate LST retrieval \(Simó et al., 2018;](#)  
524 [Li et al., 2013\)](#). After all, LST is an indirect measurement and the results of complicated mathematical processing  
525 [requiring knowledge of several components, where error in any of them causes inaccuracies in LST \(Simó et al., 2018\)](#).

526 Estimation of land surface emissivity is determinant in the correct LST retrieval, yet highly difficult to measure and prone  
527 to error. Moreover, in dense canopies the signal constitutes mostly of the upper canopy and does not necessarily capture  
528 the temperatures on the forest floor, which may not make LST representative of understory conditions (Bense et al., 2016;  
529 Zellweger et al., 2019). Landsat 8 TIRS band 11 was not used in this study due to the stray light problem, which exposes  
530 even higher possibility of inaccuracy with LST. However, Wang et al. (2019) conclude that the SC is a valid method for  
531 Landsat 8 processing and produces results on accuracy high enough for most purposes. Moreover, in dense canopies the  
532 signal constitutes mostly of the upper canopy (Bense et al., 2016; Zellweger et al., 2019), and previous studies have not  
533 so far demonstrated LST's relationship with understory conditions. We showed how LST provided consistent results with  
534 particularly  $T_{\text{surface}}$  and  $T_{\text{air}}$ . Therefore, this study contributed to clarifying the relationship of upper canopy and the  
535 understory.

536 ~~Our~~Despite its limitations, this study provided information about a topic of which importance has only recently been  
537 recognized (De Frenne et al., 2013; Jucker et al., 2018; [Davis et al., 2019](#); Zellweger et al., 2020). Research and modelling  
538 of climate change implications on microclimate cannot rely on observations from weather stations with low spatial  
539 resolution, but need data that represent the microclimatic conditions relevant for most ecosystem functions ([Potter et al.,](#)  
540 [2013](#)). Previous research about vegetation and LST have been often conducted at much lower spatial resolutions and  
541 applied less accurate topographic correction (Li et al., 2015). Furthermore, the effect of trees on climate is usually studied  
542 solely based on comparison between forest and open land (De Frenne et al., 2019), neglecting the intermediate canopies  
543 and their significance, despite of the fact that human activity focuses mostly in areas with TOF. We used microclimate  
544 data covering a CC gradient and satellite-derived LST data combined with a DEM of 30 m acquired with ALS over the  
545 versatile ~~and precise~~ study area. While establishing field observation networks with wide spatial coverage remains a  
546 challenge, our results showed that LST can be used as a proxy for assessing the impacts of CC on microclimate.

547 Future research should further investigate the contribution of varied factors to microclimate. For example, since all trees  
548 are not of equal benefits in agroforestry, more studies could be targeted to the comparison of different agroforestry  
549 species' cooling potential as well as the potential of plantation forests. Including soil moisture, air temperature and  
550 comprehensive field plot networks under different canopy structures in the future analyses should broaden the knowledge  
551 about trees' role in mitigating and adapting to climate change.

552

## 553 5. Conclusions

554 Our results demonstrate a consistent but heterogeneous influence of canopy cover on the microclimate of highly diverse  
555 tropical ecosystems. Daytime temperatures correlated inversely with canopy cover, the effect being strongest on surface  
556 temperatures. [During the hottest days in hotter environments](#), the difference between sites of high and low canopy cover  
557 became most notable. The cooling effect did not exist only with high canopy cover, but even intermediate canopy cover  
558 and trees outside forest buffered the hottest temperatures. Our results thus provide robust evidence that any efforts in the  
559 direction of preserving, restoring or increasing vegetation cover can have a substantial impact in creating more stable and  
560 cooler microclimates. Satellite-based [land surface temperature-LST](#) was a suitable proxy for assessing microclimatic  
561 variables surface- and near-ground temperatures, particularly in heterogeneous regions, where the network of field  
562 measurements cannot cover the spatial microclimate variability.

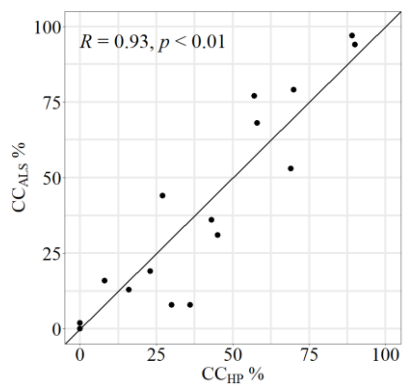
563 This study provided valuable information about the potential of trees in climate change adaptation and mitigation in  
564 tropical environments. As the effect of canopy cover on microclimate increased at lower elevations and during hot days,  
565 our results indicate that warmer and drier regions are likely to benefit the most from trees.



566 **Appendix A. Method for hemispherical photography**

567 We took hemispherical photographs at every microclimate sensor site. The camera in use was Nikon D5000 DSLR and  
568 the lens Sigma 4.5 mm F2.8 EX DC HSM Circular Fisheye. The camera was attached to a tripod during the taking of  
569 photographs. We took photographs at two different heights: the lowest possible tripod adjustment to be as close to the  
570 actual sensor level as possible, which was around 60 cm, and at eye-level around 130 cm. We took photographs at eye-  
571 level also to every intercardinal direction 15 meters away from the sensor. The camera was adjusted looking upward with  
572 the top of the camera pointing north. Two images at every height and direction were taken with different settings: first  
573 image on Program mode with automatic aperture and shutter speed, and the second on Manual mode with the rest of the  
574 settings staying the same as in picture one, except shutter speed was reduced to half of the first mage. The ISO value was  
575 set as constant 500. The purpose of the smaller shutter speed was to reduce the impact of light conditions that were not  
576 optimal, meaning direct sunlight that causes overexposure of images which in turn makes them difficult to analyze.  
577 Optimally, the photographs should be taken under constant cloud cover or at the dawn or dusk (Pellikka et al., 2000),  
578 however due to the timetable, waiting for better light conditions at some sites was not possible, thus some images were  
579 overexposed.

580  
581 We analyzed the hemispherical photographs in the software Hemisfer (WSL; version 2.2) (Schleppi et al., 2007;  
582 Thimonier et al., 2010). From the two images, we used the less exposed one in the analysis. For the calculation of canopy  
583 cover, we used the images taken from eye-level, because they were more comparable to the ALS-based canopy cover,  
584 and the photographs in cardinal directions were all taken at eye-level. We classified the image pixels to sky and canopy  
585 by determining a threshold value to separate dark and light pixels in the image. For most images, we used the automatic  
586 threshold method by Nobis and Hunziker (2005). In the case of some images, the algorithm clearly produced errors due  
587 to overexposure and direct sunlight, therefore the algorithm by Ridler and Calvart (1978) was applied, or a manual  
588 threshold was determined. We used only the blue band in the analysis, apart from photographs where the classification  
589 was failing and using all the bands produced the best result (Heiskanen et al., 2015a). The gamma correction was  $\gamma = 2.2$ .  
590 Only the zenith angle range of 0-15° was analyzed, because errors in canopy cover accuracy increase with larger angles  
591 (Paletto and Tosi, 2009). We computed canopy cover by calculating an average of 1-gap fraction of the five  
592 measurements, and this gave a plot-wise canopy cover (Heiskanen, et al., 2015b). Finally, we compared the canopy cover  
593 retrieved from hemispherical photography and ALS using Pearson's correlation and a Student's t-test. [The mean of](#)  
594 [differences was 0.89 and was not statistically significant.](#)



595

596 **Figure A1.** Comparison of canopy cover (CC) percentage retrieved from airborne laser scanning (ALS) and hemispherical  
597 photography (HP), with line of identity.

**Appendix B. Results of the linear regression models of land surface temperature.**

Predictor	Model	Coef	Std. Error	T-Value	P-Value
Constant	1	44.79	0.013	3324.0	<0.001*
	2	44.24	0.019	2300.9	<0.001*
	3	46.71	0.018	2580.3	<0.001*
	4	44.08	0.021	2130.9	<0.001*
Elevation	1	-0.013	0.000	-1241.4	<0.001*
	2	-0.011	0.000	-577.2	<0.001*
	3	-0.015	0.000	-954.6	<0.001*
	4	-0.012	0.000	-592.3	<0.001*
Slope	1	-4.061	0.018	-220.0	<0.001*
	2	-3.806	0.018	-214.9	<0.001*
	3	-3.723	0.018	-202.3	<0.001*
	4	-1.545	0.054	-28.534	<0.001*
Canopy cover	1	-0.050	0.000	-419.0	<0.001*
	2	-0.068	0.000	-449.1	<0.001*
	3	-0.109	0.000	-274.7	<0.001*
	4	-0.068	0.000	-452.4	<0.001*
NE	1	0.177	0.011	16.0	<0.001*
	2	0.084	0.010	8.1	<0.001*
	3	0.157	0.011	14.3	<0.001*
	4	-0.148	-0.016	-9.4	<0.001*
E	1	-0.030	0.010	-29.0	<0.001*
	2	-0.428	0.010	-44.6	<0.001*
	3	-0.352	0.010	-34.7	<0.001*
	4	-0.452	0.016	-32.4	<0.001*
SE	1	-1.447	0.010	-140.0	<0.001*
	2	-1.509	0.010	-155.6	<0.001*

	<u>3</u>	<u>-1.529</u>	<u>0.010</u>	<u>-149.3</u>	<u>&lt;0.001*</u>
	<u>4</u>	<u>-1.178</u>	<u>0.014</u>	<u>-85.4</u>	<u>&lt;0.001*</u>
<u>S</u>	<u>1</u>	<u>-2.095</u>	<u>0.011</u>	<u>-189.4</u>	<u>&lt;0.001*</u>
	<u>2</u>	<u>-2.132</u>	<u>0.010</u>	<u>-205.2</u>	<u>&lt;0.001*</u>
	<u>3</u>	<u>-2.186</u>	<u>0.011</u>	<u>-199.4</u>	<u>&lt;0.001*</u>
	<u>4</u>	<u>1.543</u>	<u>0.014</u>	<u>-107.3</u>	<u>&lt;0.001*</u>
<u>SW</u>	<u>1</u>	<u>-2.441</u>	<u>0.011</u>	<u>-230.0</u>	<u>&lt;0.001*</u>
	<u>2</u>	<u>-2.554</u>	<u>0.010</u>	<u>-256.0</u>	<u>&lt;0.001*</u>
	<u>3</u>	<u>-2.527</u>	<u>0.011</u>	<u>-240.1</u>	<u>&lt;0.001*</u>
	<u>4</u>	<u>-1.820</u>	<u>0.014</u>	<u>-130.2</u>	<u>&lt;0.001*</u>
<u>W</u>	<u>1</u>	<u>-2.293</u>	<u>0.010</u>	<u>-219.5</u>	<u>&lt;0.001*</u>
	<u>2</u>	<u>-2.254</u>	<u>0.010</u>	<u>-229.9</u>	<u>&lt;0.001*</u>
	<u>3</u>	<u>-2.332</u>	<u>0.010</u>	<u>-225.5</u>	<u>&lt;0.001*</u>
	<u>4</u>	<u>-1.554</u>	<u>0.014</u>	<u>-109.2</u>	<u>&lt;0.001*</u>
<u>NW</u>	<u>1</u>	<u>-1.380</u>	<u>0.011</u>	<u>-126.8</u>	<u>&lt;0.001*</u>
	<u>2</u>	<u>-1.205</u>	<u>0.010</u>	<u>-117.9</u>	<u>&lt;0.001*</u>
	<u>3</u>	<u>-1.379</u>	<u>0.012</u>	<u>-127.9</u>	<u>&lt;0.001*</u>
	<u>4</u>	<u>-0.883</u>	<u>0.015</u>	<u>-58.5</u>	<u>&lt;0.001*</u>
<u>1000-1500 m</u>	<u>1</u>	±	±	±	±
	<u>2</u>	<u>-2.667</u>	<u>0.008</u>	<u>-346.9</u>	<u>&lt;0.001*</u>
	<u>3</u>	±	±	±	±
	<u>4</u>	<u>-2.645</u>	<u>0.008</u>	<u>-346.8</u>	<u>&lt;0.001*</u>
<u>&gt;1500 m</u>	<u>1</u>	±	±	±	±
	<u>2</u>	<u>-2.030</u>	<u>0.018</u>	<u>-111.2</u>	<u>&lt;0.001*</u>
	<u>3</u>	±	±	±	±
	<u>4</u>	<u>-1.875</u>	<u>0.018</u>	<u>-103.5</u>	<u>&lt;0.001*</u>
<u>Canopy cover: 1000–1500 m</u>	<u>1</u>	±	±	±	±
	<u>2</u>	<u>0.031</u>	<u>0.000</u>	<u>149.7</u>	<u>&lt;0.001*</u>
	<u>3</u>	±	±	±	±

	<u>4</u>	<u>0.031</u>	<u>0.000</u>	<u>151.2</u>	<u>&lt;0.001*</u>
	<u>1</u>	±	±	±	±
<u>Canopy cover:</u>	<u>2</u>	<u>0.028</u>	<u>0.000</u>	<u>120.7</u>	<u>&lt;0.001*</u>
<u>&gt;1500m</u>	<u>3</u>	±	±	±	±
	<u>4</u>	<u>0.038</u>	<u>0.000</u>	<u>122.5</u>	<u>&lt;0.001*</u>
	<u>1</u>	±	±	±	±
<u>Elevation: canopy</u>	<u>2</u>	±	±	±	±
<u>cover</u>	<u>3</u>	<u>0.00005</u>	<u>0.000</u>	<u>156.3</u>	<u>&lt;0.001*</u>
	<u>4</u>	±	±	±	±
	<u>1</u>	±	±	±	±
<u>Slope: NE</u>	<u>2</u>	±	±	±	±
	<u>3</u>	±	±	±	±
	<u>4</u>	<u>0.798</u>	<u>0.062</u>	<u>11.8</u>	<u>&lt;0.001*</u>
	<u>1</u>	±	±	±	±
<u>Slope: E</u>	<u>2</u>	±	±	±	±
	<u>3</u>	±	±	±	±
	<u>4</u>	<u>-0.144</u>	<u>0.060</u>	<u>-2.387</u>	<u>0.017</u>
	<u>1</u>	±	±	±	±
<u>Slope: SE</u>	<u>2</u>	±	±	±	±
	<u>3</u>	±	±	±	±
	<u>4</u>	<u>-2.014</u>	<u>0.061</u>	<u>-33.1</u>	<u>&lt;0.001*</u>
	<u>1</u>	±	±	±	±
<u>Slope: S</u>	<u>2</u>	±	±	±	±
	<u>3</u>	±	±	±	±
	<u>4</u>	<u>-4.045</u>	<u>0.067</u>	<u>-60.0</u>	<u>&lt;0.001*</u>
	<u>1</u>	±	±	±	±
<u>Slope: SW</u>	<u>2</u>	±	±	±	±
	<u>3</u>	±	±	±	±
	<u>4</u>	<u>-0.943</u>	<u>0.063</u>	<u>-78.1</u>	<u>&lt;0.001*</u>

<u>Slope: W</u>	<u>1</u>	±	±	±	±
	<u>2</u>	±	±	±	±
	<u>3</u>	±	±	±	±
	<u>4</u>	<u>-3.918</u>	<u>0.060</u>	<u>-64.8</u>	<u>&lt;0.001*</u>
<u>Slope: NW</u>	<u>1</u>	±	±	±	±
	<u>2</u>	±	±	±	±
	<u>3</u>	±	±	±	±
	<u>4</u>	<u>-1.963</u>	<u>0.065</u>	<u>-30.4</u>	<u>&lt;0.001*</u>

599

600 **Table B1:** Summary of regression coefficients in the analysis of land surface temperature (LST) from the four models

601 tested. \* indicates statistical significance.

602 **Data and code availability**

603 The data and scripts presented in this study are available on request from the author (I.A.).

604 **Author contribution**

605 Conceptualization, I.A., E.M., J.H. and P.P.; data curation, I.A.; formal analysis, I.A., E.A.; funding acquisition, P.P.;  
606 investigation, I.A., methodology, I.A, E.M., J.H., E.A. and P.P.; project administration, E.M. and P.P.; resources,  
607 software, I.A.; supervision, E.M, J.H. and P.P.; validation, I.A., visualization, I.A., writing—original draft preparation,  
608 I.A.; writing—review and editing, IA., E.M., J.H. and P.P. All authors have read and agreed to the published version of  
609 the manuscript.

610 **Declaration of Competing Interest**

611 The authors declare that they have no conflicts of interest.

612 **Funding**

613 This study was conducted as part of Smartland project (Environmental sensing of ecosystem— services for developing a  
614 climate-smart landscape framework to improve food security in East Africa, decision no. 31864) funded by Academy of  
615 Finland, and ESSA project (Earth observation and environmental sensing for climate-smart sustainable agropastoral  
616 ecosystem transformation in East Africa) funded by European Commission DG International Partnerships DeSIRA  
617 programme (FOOD/2020/418-132). Eduardo Maeda was funded by the Academy of Finland (decision numbers 318252  
618 and 319905).

619 **Acknowledgements**

620 We would like to acknowledge Agnes Mwangombe, Ali Ndizi, Mrs. Mwamburis, Mrs. Nyatta, Cathrine Mwakesi, Simon,  
621 Moses Onyimbo and Dalmas moka secondary school, Jason Collette and Teita Sisal Estate, St. Mary’s Teachers’ Training  
622 College, and Taita Taveta University Ngerenyi campus for allowing us to conduct this research on their properties. We  
623 also thank Taita Research Station of the University of Helsinki for logistical support during the field wok campaign.  
624 Special thanks to Mwadime Mjomba for assistance during the field work. We acknowledge Matti Räsänen for the  
625 provision of weather station data and Hari Adhikari for the canopy cover data. [We also want to thank the two anonymous](#)  
626 [reviewers for their comments and suggestions to improve the manuscript.](#)

627

628 **References**

629 Abdelgalil, E. A.: Deforestation in the drylands of Africa: Quantitative modelling approach, *Environment, Development*  
630 *and Sustainability*, 6, 415–427, <http://dx.doi.org/10.1007/s10668-005-0787-1>, 2004.

631 Abera, T. A., Heiskanen, J., Pellikka, P. K., Adhikari, H., and Maeda, E. E.: Climatic impacts of bushland to cropland  
632 conversion in Eastern Africa, *Sci. Total. Environ.*, 717,

633 <https://doi.org/10.1016/j.scitotenv.2020.137255><https://doi.org/10.1016/j.scitotenv.2020.137255>, 2020.

**Formatted:** Graduteksti Char, Font: 10 pt

634 Adhikari, H., Heiskanen, J., Siljander, M., Maeda, E., Heikinheimo, V., and Pellikka, P. K.: Determinants of  
635 Aboveground Biomass across an Afromontane Landscape Mosaic in Kenya, *Remote Sens.*, 9, 827,

636 <https://doi.org/10.3390/rs9080827><https://doi.org/10.3390/rs9080827>, 2017.

**Field Code Changed**

637 Adhikari, U., Nejadhashemi, A. P., and Woznicki, S. A.: Climate change and eastern Africa: a review of impact on  
638 major crops, *Food and Energy Security*, 4, 110–132. <http://dx.doi.org/10.1002/fes3.61>, 2015.

**Field Code Changed**

639 Agriculture (Farm Forestry) Rules, 2009 (Cap. 318) (KEN).

640 Allen, R. G., Pereira, L. S., Raes, D., and Smith, M.: Crop evapotranspiration - Guidelines for computing crop water  
641 requirements, Food and Agriculture Organization of the United Nations, Rome, Italy, 1998

642 Amara, E., Adhikari, H., Heiskanen, J., Siljander, M., Munyao, M., Omondi, P., and Pellikka, P.: Aboveground  
643 Biomass Distribution in a Multi-Use Savannah Landscape in Southeastern Kenya: Impact of Land Use and Fences,  
644 *Land*, 9, 381, <https://doi.org/10.3390/land9100381>, 2020.

**Field Code Changed**

645 Beer, C., Reichstein, M., Tomelleri, E., Ciais, P., Jung, M., Carvalhais, N., . . . Papale, D.: Terrestrial Gross Carbon  
646 Dioxide Uptake Distribution and Covariation with Climate, *Science*, 329, 834–838,

647 <https://doi.org/10.1126/science.1184984>, 2010.

**Field Code Changed**

648 Belsky, A. J., Amundson, R. G., Duxbury, J. M., Riha, S. J., Ali, A. R., and Mwonga, S. M.: The Effects of Trees on  
649 Their Physical, Chemical and Biological Environments in a Semi-Arid Savanna in Kenya, *J. Appl. Ecol.*, 26, 1005–  
650 1024. <https://doi.org/10.2307/2403708>, 1989.

**Field Code Changed**

651 Bense, V. F., Read, T., and Verhoef, A.: Using distributed temperature sensing to monitor field scale dynamics of  
652 ground surface temperature and related substrate heat flux, *Agr. Forest. Meteorol.*, 220, 207–215.

653 <https://doi.org/10.1016/j.agrformet.2016.01.138>, 2016.

**Field Code Changed**



654 Cairns, J. E., Hellin, J., Sonder, K., Araus, J. L., MacRoberts, J. F., Thierfelder, C., and Prasanna, B. M.: Adapting  
655 maize production to climate change in sub-Saharan Africa, *Food Secur.*, 5, 345–360, [https://doi.org/10.1007/s12571-](https://doi.org/10.1007/s12571-013-0256-x)  
656 013-0256-x, 2013.

Field Code Changed

657 [Chakravarty, S., Pala, N. A., Tamang, B., Sarkar, B. C., Abna Manohar K., Rai, P., Puri, A., and Shukla, G.: Ecosystem  
658 services of Trees Outside Forest. in: Sustainable Agriculture. Forest and Environmental Management, edited by:  
659 Jhariya, M. K., Banerjee, A., Meena, R. S., and Yadav, D. K. Springer, \[https://doi.org/10.1007/978-981-13-6830-1\\\_10\]\(https://doi.org/10.1007/978-981-13-6830-1\_10\),  
660 2019.](#)

661 Chen, J., Saunders, S. C., Crow, T. R., and Naiman, R. J.: Microclimate in forest ecosystem and landscape ecology,  
662 *Bioscience*, 49, 288–297, <http://dx.doi.org/10.2307/1313612>, 1999.

Field Code Changed

663 Das, A., Nagendra, H., Anand, M., and Bunyan, M.: Topographic and Bioclimatic Determinants of the Occurrence of  
664 Forest and Grassland in Tropical Montane Forest-Grassland Mosaics of the Western Ghats, India, *PLoS One*, 10,  
665 e0130566, <http://dx.doi.org/10.1371/journal.pone.0130566>, 2015.

Field Code Changed

666 [Davis, K., T., Dobrowski, S. Z., Holden, Z. A., Higuera, P. E., and Abatzoglou, J. T.: Microclimate buffering in forests  
667 of the future: the role of local water balance, \*Ecography\*, 42, 1–11, <https://doi.org/10.1111/ecog.03836>, 2019.](#)

668 De Frenne, P., Rodríguez-Sánchez, F., Coomes, D. A., Baeten, L., Verstraeten, G., Vellend, M., . . . Verheyen, K.:  
669 Microclimate moderates plant responses to macroclimate warming, *P. Natl. Acad. Sci. USA.*, 110, 18561–18565,  
670 <https://doi.org/10.1073/pnas.1311190110>, 2013.

Field Code Changed

671 De Frenne, P., Zellweger, F., Rodríguez-Sánchez, F., Scheffers, B. R., Hylander, K., Luoto, M., . . . Lenoir, J.: Global  
672 buffering of temperatures under forest canopies, *Nat. Ecol. Evol.*, 3, 744–749, [http://dx.doi.org/10.1038/s41559-019-](http://dx.doi.org/10.1038/s41559-019-0842-1)  
673 0842-1, 2019.

Field Code Changed

674 [De Frenne, P., Lenoir, J., Luoto, M., Scheffers, B. R., Zellweger, F., Aalto, J., . . . Hylander, K.: Forest microclimates  
675 and climate change: Importance, drivers and future research agenda, \*Glob Chang Biol.\*, 27, 2279–2297,  
676 <https://doi.org/10.1111/gcb.15569>, 2021.](#)

677 Ellison, D., Morris, C. E., Locatelli, B., Sheil, D., Cohen, J., Murdiyarsa, D., . . . Sullivan, C. A.: Trees, forests and  
678 water: Cool insights for a hot world, *Global Environ. Chang.*, 43, 51–61,  
679 <https://doi.org/10.1016/j.gloenvcha.2017.01.002>, 2017.

Field Code Changed

680 Erdogan, H. E., Pellikka, P. K., and Clark, B.: Modelling the impact of land-cover change on potential soil loss in the  
681 Taita Hills, Kenya, between 1987 and 2003 using remote-sensing and geospatial data, *Int. J. Remote Sens.*, 32, 5919–  
682 5945, <https://doi-org.ftp.proxy.helsinki.fi/10.1080/01431161.2010.499379>, 2011.

683 Ewers, R. M., and Banks-Leite, C.: Fragmentation Impairs the Microclimate Buffering Effect of Tropical Forests, *PLoS*  
684 *One*, 8, e58093, <https://doi.org/10.1371/journal.pone.0058093>, 2013.

685 FAO: Global Forest Resources Assessment 2000 (FRA 2000). Food and Agriculture Organization of the United  
686 Nations, Rome, Italy, 2000.

687 FAO: Forest Resources Assessment. Terms and definitions. Food and Agriculture Organization of the United Nations,  
688 Rome, Italy, 2015.

689 FAO: Global forest resources assessment 2015. How are the world's forests changing? (2 ed.), Food and Agriculture  
690 Organization of the United Nations, Rome, Italy, 2016.

691 [Geiger, R.: The climate near the ground, 4<sup>th</sup> edition, Harvard University Press, United States of America, 1980.](#)

692 [Goward, S. N., Cruickshanks, G. D., and Hope, A. S.: Observed relation between thermal emission and reflected spectral](#)  
693 [radiance of a complex vegetated landscape, \*Remote Sens. Environ.\*, 18, 137–146, 1985.](#)

694 [Goward, S. N., and Hope, A. S.: Evapotranspiration from combined reflected solar and emitted terrestrial radiation:](#)  
695 [Preliminary FIFE results from AVHRR data, \*Adv. Space Res.\*, 9, 239–249, 1989.](#)

696 Griffin, A. M., Popescu, S. C., and Zhao, K.: Using LIDAR and Normalized Difference Vegetation Index to remotely  
697 determine LAI and percent canopy cover, in: *SilviLaser*, Edinburgh, United Kingdom, 17–19 September, 446–455,  
698 2008.

699 He, J., Zhao, W., Li, A., Wen, F., and Yu, D.: The impact of the terrain effect on land surface temperature variation  
700 based on Landsat-8 observations in mountainous areas, *Int. J. Remote Sens.*, 40, 1808–1827,  
701 <https://doi.org/10.1080/01431161.2018.1466082>, 2019.

702 Heiskanen, J., Korhonen, L., Hietanen, J., and Pellikka, P. K.: Use of airborne lidar for estimating canopy gap fraction  
703 and leaf area index of tropical montane forests, *Int. J. Remote Sens.*, 36, 2569–2583,  
704 <https://doi.org/10.1080/01431161.2015.1041177>, 2015a.

Field Code Changed

Field Code Changed

Field Code Changed

705 Heiskanen, J., Korhonen, L., Hietanen, J., Heikinheimo, V., Schäfer, E., and Pellikka, P. K. E.: Comparison of field and  
706 airborne laser scanning based crown cover estimates across land cover types in Kenya, *Int. Arch. Photogramm. Remote*  
707 *Sens. Spatial Inf. Sci.*, XL-7/W3, 409–415, <https://doi.org/10.5194/isprsarchives-XL-7-W3-409-2015>, 2015b.

Field Code Changed

708 Helle, J.: Lentolaserkeilaus ja hemisfäärikuvaus metsikkösadannan tutkimisessa Taitavuorilla Keniassa, B.Sc. thesis,  
709 University of Helsinki, 2016.

710 [Iiyama, M., Neufeldt, H., Dobie, P., Njenga, M., Ndegwa, G., and Jamnadass, R.: The potential of agroforestry in the](#)  
711 [provision of sustainable woodfuel in sub-Saharan Africa, \*Curr. Opin. Environ. Sustain.\*, 6, 138–147,](#)  
712 <https://doi.org/10.1016/j.cosust.2013.12.003>, 2014

713

714 IPCC: Global Warming of 1.5°C. An IPCC Special Report on the impacts of global warming of 1.5°C above pre-  
715 industrial levels and related global greenhouse gas emission pathways, in the context of strengthening the global  
716 response to the threat of climate change, sustainable development, and efforts to eradicate poverty, Intergovernmental  
717 Panel on Climate Change, 2018.

718 Jiménez-Muñoz, J. C., and Sobrino, J. A.: A generalized single-channel method for retrieving land surface temperature  
719 from remote sensing data, *J. Geophys. Res.*, 108, 4688, <https://doi.org/10.1029/2003JD003480>, 2003.

720 Jiménez-Muñoz, J. C., Sobrino, J. A., Skoković, D., Mattra, C., and Cristóbal, J.: Land Surface Temperature Retrieval  
721 Methods from Landsat-8 Thermal Infrared Sensor Data. *IEEE Geosci. Remote S.*, 11, 1840–1843,  
722 <https://doi.org/10.1109/LGRS.2014.2312032>, 2014.

723 Jin, M., and Dickinson, R. E.: Land surface skin temperature climatology: benefitting from the strengths of satellite  
724 observations, *Environ. Res. Lett.*, 5, <https://doi.org/10.1088/1748-9326/5/4/044004>, 2010.

725 Jucker, T., Hardwick, S. R., Both, S., Elias, D. D., Ewers, R. M., Milodowski, D. T. . . . Coomes, D. A.: Canopy  
726 structure and topography jointly constrain the microclimate of human-modified tropical landscapes, *Glob. Change Biol.*,  
727 24, 5243–5258, <https://doi.org/10.1111/gcb.14415>, 2018.

728 Kim, J.-P.: Variation in the accuracy of thermal remote sensing, *Int. J. Remote Sens.*, 34, 729–750,  
729 <https://doi.org/10.1080/01431161.2012.713143>, 2013.

Field Code Changed

730 Korhonen, L., Korhonen, K. T., Rautiainen, M., and Stenberg, P.: Estimation of Forest Canopy Cover: A Comparison of  
731 Field Measurement Techniques, *Silva Fenn.*, 40, 577–588, <https://doi.org/10.14214/sf.315>, 2006.

Field Code Changed

732 [Kuyah, S., Whitney, C. W., Jonsson, M., Sileshi, G. W., Öborn, I., Muthuri, C. W., & Luedeling, E. \(2019\). Agroforestry](#)  
733 [delivers a win-win solution for ecosystem services in sub-Saharan Africa. A meta-analysis. \*Agron Sustain Dev\*, 39,](#)  
734 <https://doi.org/10.1007/s13593-019-0589-8>, 2019.

735 [Lee, X., Goulden, M. L., Hollinger, D. Y., Barr, A., Black, T. A., Bohrer, G., . . . Zhao, L.: Observed increase in local](#)  
736 [cooling effect of deforestation at higher latitudes. \*Nature\* 479, 384–387, https://doi.org/10.1038/nature10588](#), 2011.

737 Li, Y., Zhao, M., Motesharrei, S., Mu, Q., Kalnay, E., and Li, S.: Local cooling and warming effects of forests based on  
738 satellite observations, *Nature Communications*, 6, <http://dx.doi.org/10.1038/ncomms7603>, 2015.

739 Li, Y., De Noblet-Ducoudré, N., Davin, E. L., Motesharrei, S., Zeng, N., Li, S., and Kalnay, E.: The role of spatial scale  
740 and background climate in the latitudinal temperature response to deforestation, *Earth Syst. Dynam.*, 7, 167–181,  
741 <https://doi.org/10.5194/esd-7-167-2016>, 2016.

742 Li, Z.-L., Tang, B.-H., Wu, H., Ren, H., Yan, G., Wan, Z., . . . Sobrino, J. A.: Satellite-derived land surface temperature:  
743 Current status and perspectives. *Remote Sens. Environ.*, 131, 14–37, <https://doi.org/10.1016/j.rse.2012.12.008>, 2013.

744 Luyssaert, S., Jammot, M., Stoy, P. C., Estel, S., Pongratz, J., Ceschia, E., . . . Dolman, A. J.: Land management and land-  
745 cover change have impacts of similar magnitude on surface temperature, *Nat. Clim. Change*, 4, 389–393, <http://dx.doi.org>-.  
746 <libproxy.helsinki.fi/10.1038/nclimate2196>, 2014.

747 [Mace, G. M., Norris, K. and Fitter, A. H.: Biodiversity and ecosystem services: a multilayered relationship, \*Trends Ecol\*](#)  
748 [Evol. 27, 19–26, https://doi.org/10.1016/j.tree.2011.08.006](#), 2012.

749 [Maclean, Duffy, J. P., Haesen, S., Govaert, S., De Frenne, P., Vanneste, T., Lenoir, J., Lembrechts, J. J., Rhodes, M. W.,](#)  
750 [& Van Meerbeek, K.: On the measurement of microclimate. \*Methods Ecol. Evol.\*, 12, 1397–1410,](#)  
751 <https://doi.org/10.1111/2041-210X.13627>, 2021.

752 Maeda, E. E., and Hurskainen, P.: Spatiotemporal characterization of land surface temperature in Mount Kilimanjaro  
753 using satellite data, *Theor. Appl. Climatol.*, 118, 497–509, <http://doi.org/10.1007/s00704-013-1082-y>, 2014.

754 Maeda, E. E., Clark, B. J., Pellikka, P., and Siljander, M.: Modelling agricultural expansion in Kenya’s Eastern Arc  
755 Mountains biodiversity hotspot, *Agr. Syst.*, 103, 609–620, <http://dx.doi.org/10.1007/s00704-013-1082-y>, 2010.

756 Martínez Pastur, G., Perera, A. H., Peterson, U., and Iverson, L. R.: Ecosystem Services from Forest Landscapes: An  
757 Overview, in: *Ecosystem Services from Forest Landscape*, edited by: Perera, A., Peterson, U., Pastur, G., and Iverson,  
758 L. Springer, <https://doi.org/10.1007/978-3-319-74515-2>, 2018.

Field Code Changed

Field Code Changed

Field Code Changed

Field Code Changed

Field Code Changed

759 Mendenhall, C. D., Shields-Estrada, A., Krishnaswami, A. J., and Daily, G. C.: Quantifying and sustaining biodiversity  
760 in tropical agricultural landscapes, *P. Natl. Acad. Sci. USA*, 113, 14544–14551, [https://doi-](https://doi-<br/>761 org/10.1073/pnas.1604981113)

Field Code Changed

762 Mildrexler, D. J., Zhao, M., and Running, S. W.: A global comparison between station air temperatures and MODIS  
763 land surface temperatures reveals the cooling role of forests, *J. Geophys. Res.*, 116,  
764 <https://doi.org/10.1029/2010JG001486>, 2011.

Field Code Changed

765 MoALF: Climate Risk Profile for Taita Taveta. Kenya County Climate Risk Profile Series, The Kenya Ministry of  
766 Agriculture, Livestock and Fisheries (MoALF), Nairobi, 2016.

767 Muimba-Kankolongo, A.: Food Crop Production by Smallholder Farmers in Southern Africa, Academic Press, pp. 382,  
768 2018.

769 Mwalusepo, S., Massawe, E. S., Affognon, H., Okuku, G. O., Kingori, S., Mburu, P. D., . . . Le Ru, B. P.: Smallholder  
770 Farmers' Perspectives on Climatic Variability and Adaptation Strategies in East Africa: The Case of Mount Kilimanjaro  
771 in Tanzania, Taita and Machakos Hills in Kenya, *J. Earth Sci. Clim. Change*, 6, [http://dx.doi.org/10.4172/2157-](http://dx.doi.org/10.4172/2157-<br/>772 7617.1000313)

Field Code Changed

773 Ndossi, M. I., and Avdan, U.: Application of Open Source Coding Technologies in the Production of Land Surface  
774 Temperature (LST) Maps from Landsat: A PyQGIS Plugin, *Remote Sens.*, 8, 413. <https://doi.org/10.3390/rs8050413>,  
775 2016.

Field Code Changed

776 Nemani, R., Pierce, L., and Running, S.: Developing Satellite-derived Estimates of Surface Moisture Status, *J. Appl.*  
777 *Meteorol.*, 32, 548–557, 1993.

778 [Nemani, R. R., and Running, S. W.: Land cover characterization using multitemporal red, near-IR, and thermal-IR data  
779 from NOAA/AVHRR, \*Ecol. Appl.\*, 7, 79–90, 1997.](#)

780 [Nyamadzawo G., Nyamugafata P., Chikowo R., Giller K. E.: Partitioning of simulated rainfall in a kaolinitic soil under  
781 improved fallow-maize rotation in Zimbabwe, \*Agrofor Syst.\*, 59, 207–214,  
782 <https://doi.org/10.1023/B:AGFO.0000005221.67367.fd>, 2003.](#)

783 [Nyamadzawo G., Chikowo R., Nyamugafata P., Giller K. E.: Improved legume tree fallows and tillage effects on  
784 structural stability and infiltration rates of a kaolinitic sandy soil from central Zimbabwe, \*Soil Tillage Res.\*, 96, 182–194,  
785 <https://doi.org/10.1016/j.still.2007.06.008>, 2007.](#)

786 [Nyamadzawo G., Nyamugafata P., Wuta M., Nyamangara J.: Maize yields under coppicing and non coppicing fallows](#)  
787 [in a fallow-maize rotation system in central Zimbabwe. \*Agrofor Syst.\* 84, 273–286. \[9453-9, 2012.\]\(https://doi.org/10.1007/s10457-011-</a></a><br/>788 <a href=\)](#)

789 Ong, C. K., Black, C. R., and Muthuri, C. W.: Modifying forestry and agroforestry to increase water productivity, CAB  
790 Reviews: Perspectives in Agriculture, Veterinary Science, Nutrition and Natural Resources, 1,  
791 <https://doi.org/10.1079/PAVSNNR20061065>, 2006.

Field Code Changed

792 Pellikka, P., and Hakala, E.: Climate change, in: Megatrends in Africa, edited by: Vastapuu, I., Mattlin, M., Hakala, E.,  
793 and Pellikka, P., 7–14, Ministry of Foreign Affairs of Finland, 2019.

794 Pellikka, P. K., Lötjönen, M., Siljander, M., and Lens, L.: Airborne remote sensing of spatiotemporal change (1955–  
795 2004) in indigenous and exotic forest cover in the Taita Hills, Kenya, *Int. J. Appl. Earth Obs.*, 11, 221–232,  
796 <https://doi.org/10.1016/j.jag.2009.02.002>, 2009.

Field Code Changed

797 Pellikka, P. K., Clark, B. J., Gosa, A. G., Himberg, N., Hurskainen, P., Maeda, E., . . . Siljander, M.: Agricultural  
798 Expansion and Its Consequences in the Taita Hills, Kenya, in: *Developments in Earth Surface Processes*, Vol. 16, edited  
799 by: Paron, P., Olago, D., and Omuto, C.T., Elsevier, Amsterdam, 165–179, 2013.

800 Pellikka, P. K., Heikinheimo, V., Hietanen, J., Schäfer, E., Siljander, M., and Heiskanen, J.: Impact of land cover  
801 change on aboveground carbon stocks in Afromontane landscape in Kenya, *Appl. Geogr.*, 94, 178–189,  
802 <https://doi.org/10.1016/j.apgeog.2018.03.017>, 2018.

Field Code Changed

803 Potter, K. A., Woods, H. A., and Pincebourde, S.: Microclimatic challenges in global change biology, *Glob. Change*  
804 *Biol.*, 19, 2932–2939, <https://doi.org/10.1111/gcb.12257>, 2013.

Field Code Changed

805 Prata, A. J., Caselles, V., Coll, C., Sobrino, A., and Ottlé, C.: Thermal Remote Sensing of Land Surface Temperature  
806 from Satellites: Current Status and Future Prospects, *Remote Sensing Reviews*, 12, 175–224,  
807 <https://doi.org/10.1080/02757259509532285>, 1995.

Field Code Changed

808 R Core Team: RStudio: Integrated Development for R. RStudio, PBC, Boston, United States: <http://www.rstudio.com/>,  
809 2019.

Field Code Changed

810 [Rhoades, C.: Seasonal pattern of nitrogen mineralization and soil moisture beneath \*Faidherbia albida\* \(syn \*Acacia albida\*\)](#)  
811 [in central Malawi. \*Agrofor Syst.\* 29, 133–145, 1995.](#)

812 Räsänen, M., Chung, M., Katurji, M., Pellikka, P., Rinne, J., and Katul, G. G.: Similarity in Fog and Rainfall  
813 Intermittency, *Geophys. Res. Lett.*, 45, 10691–10699, 2018.

814 Simó, G., Martínez-Villagrasa, D., Jiménez, M. A., and Cuxart, J.: Impact of the Surface–Atmosphere Variables on the  
815 Relation between Air and Land Surface Temperatures, *Pure Appl. Geophys.*, 175, 3939–3953,  
816 <https://doi.org/10.1007/s00024-018-1930-x>, 2018.

Field Code Changed

817 [Skole, D. L., Mbow, C., Mugabowindekwe, M., Brandt, M. S., and Samek, J. H.: Trees outside forests as natural](#)  
818 [climate solutions, \*Nat. Clim. Chang.\*, 11, 1013–1016, <https://doi.org/10.1038/s41558-021-01230-3>, 2021.](#)  
819 [Siriri, D., Wilson, J., Coe, R., Tenywa, M. M., Bekunda, M. A., Ong, C. K. and Black, C. R.: Trees improve water storage](#)  
820 [and reduce soil evaporation in agroforestry systems on bench terraces in SW Uganda, \*Agroforest Syst.\*, 87, 45–58,](#)  
821 <https://doi.org/10.1007/s10457-012-9520-x>, 2013.

822 Thijs, K. W., Aerts, R., van der Moortele, P., Aben, J., Musila, W., Pellikka, P., Gulink, H., and Muys, B.: Trees in a  
823 human-modified tropical landscape: Species and trait composition and potential ecosystem services, *Landscape Urban*  
824 *Plan.*, 144, 49–58, <https://doi.org/10.1016/j.landurbplan.2015.07.015>, 2015.

Field Code Changed

825 Tuure, J., Korpela, A., Hautala, M., Hakojärvi, M., Mikkola, H., Räsänen, M., Duplissy, J., Pellikka, P., Kulmala, M.,  
826 Petäjä, T., and Alakukku, L.: Comparison of surface foil materials and dew collectors location in an arid area: a one-year  
827 experiment in Kenya, *Agr. Forest Meteorol.* 276–277, 107613, <https://doi.org/10.1016/j.agrformet.2019.06.012>, 2019.

828 Unruh, J. D., Houghton, R. A., and Lefebvre, P. A.: Carbon storage in agroforestry: an estimate for sub-Saharan Africa,  
829 *Clim. Res.*, 3, 39–52, 1993.

830 USGS. (2017). Landsat 8 OLI and TIRS Calibration Notices: [https://www.usgs.gov/land-resources/nli/landsat/landsat-](https://www.usgs.gov/land-resources/nli/landsat/landsat-8-oli-and-tirs-calibration-notice)  
831 [8-oli-and-tirs-calibration-notice](https://www.usgs.gov/land-resources/nli/landsat/landsat-8-oli-and-tirs-calibration-notice), last access: 17 February 2020, 2017.

Field Code Changed

832 Wachiye, S., Merbold, L., Vesala, T., Rinne, J., Räsänen, M., Leitner, S., and Pellikka, P.: Soil greenhouse gas  
833 emissions under different land-use types in savanna ecosystems of Kenya, *Biogeosciences*, 17, 2149–2167,  
834 <https://doi.org/10.5194/bg-17-2149-2020>, 2020.

Field Code Changed

835 Wanderley, R. L., Domingues, L. M., Joly, C. A., and da Rocha, H. R.: Relationship between land surface temperature  
836 and fraction of anthropized area in the Atlantic forest region, Brazil, *PLoS One*, 14,  
837 <http://dx.doi.org/10.1371/journal.pone.0225443>, 2019.

Field Code Changed

838 Wang, L., Lu, Y., and Yao, Y.: Comparison of Three Algorithms for the Retrieval of Land Surface Temperature from  
839 Landsat 8 Images, *Sensors*, 19, 5049, <http://dx.doi.org/10.3390/s19225049>, 2019.

840 Wild, J., Kopecký, M., Maeck, M., Sanda, M., Jankovec, J., and Haase, T.: Climate at ecologically relevant scales: A  
841 new temperature and soil moisture logger for long-term microclimate measurement, *Agr. Forest Meteorol.*, 268, 40–47,  
842 <https://doi.org/10.1016/j.agrformet.2018.12.018>, 2019.

Field Code Changed

843 Zellweger, F., De Frenne, P., Lenoir, J., Rocchini, D., and Coomes, D.: Advances in Microclimate Ecology Arising  
844 from Remote Sensing, *Trends Ecol. Evol.*, 34, 327–341, <https://doi.org/10.1016/j.tree.2018.12.012>, 2019.

Field Code Changed

845 Zellweger, F., De Frenne, P., Lenoir, J., Vangansbeke, P., Verheyen, K., Bernhardt-Römermann, M., . . . Coomes, D.:  
846 Forest microclimate dynamics drive plant responses to warming, *Science*, 368, 772–775,  
847 <https://doi.org/10.1126/science.aba6880>, 2020.

Field Code Changed

848 [Zschauer K.: Households energy supply and the use of fuelwood in the Taita Hills, Kenya. MSc thesis. Department of  
849 Geosciences and Geography, University of Helsinki, Finland. 101 pp., <http://urn.fi/URN:NBN:fi-fe201201311271>, 2012.](#)

850 Zomer, R. J., Trabucco, A., Coe, R., Place, F., van Noordwijk, M., and Xu, J. C.: Trees on farms: an update and  
851 reanalysis of agroforestry's global extent and socio-ecological characteristics. Working Paper 179, World Agroforestry  
852 Centre (ICRAF) Southeast Asia Regional Program, Bogor, Indonesia, 2014.

853

#### 854 **Additional references in Appendix A:**

855 Nobis, M., and Hunziker, U.: Automatic thresholding for hemispherical canopy-photographs based on edge detection,  
856 *Agr. Forest Meteorol.*, 128, 243–250, <https://doi.org/10.1016/j.agrformet.2004.10.002>, 2005.

Field Code Changed

857 Paletto, A., and Tosi, V.: Forest canopy cover and canopy closure: comparison of assessment techniques, *Eur. J. Forest  
858 Res.*, 128, 265–272, <https://dx.doi.org/10.1007/s10342-009-0262-x>, 2009.

Field Code Changed

859 Pellikka, P., Seed, E. D., and King, D. J.: Modelling Deciduous Forest Ice Storm Damage Using Aerial CIR Imagery and  
860 Hemispheric Photography, *Can. J. Remote Sens.*, 26, 394–405, <https://doi.org/10.1080/07038992.2000.10855271>, 2000.

Field Code Changed

861 Ridler, T. W., and Calvard, S.: Picture Thresholding Using an Iterative Selection Method, *IEEE T. Syst. Man Cyb.*, 8,  
862 630–632., 1978.

863 Schleppei, P., Conedera, M., Sedivy, I., and Thimonier, A.: Correcting non-linearity and slope effects in the estimation of  
864 the leaf area index of forests from hemispherical photographs, *Agr. Forest Meteorol.*, 144, 236–242,  
865 <https://doi.org/10.1016/j.agrformet.2007.02.004>, 2007.

Field Code Changed



866 Thimonier, A., Sedivy, I., and Schleppi, P.: Estimating leaf area index in different types of mature forest stands in  
867 Switzerland: a comparison of methods, Eur. J. Forest Res., 129, 543562, <https://doi.org/10.1007/s10342-009-0353-8>,  
868 2010.

Field Code Changed